



**IMPLEMENTING MULTI-SCALE AGRICULTURAL INDICATORS EXPLOITING SENTINELS**

**VEGETATION FIELD DATA AND PRODUCTION OF GROUND-  
BASED MAPS:**

**SOUTH WEST SITE, FRANCE  
JUNE -SEPTEMBER, 2013**

**ISSUE I1.20**

EC Proposal Reference N° FP7-311766

Actual submission date : June 2014

Start date of project: 01.11.2012

Duration : 40 months

**Name of lead partner for this deliverable: EOLAB**

**Book Captain:** Jorge Sánchez(EOLAB)

Contributing Authors: Vicent Sendra (EOLAB)



Fernando Camacho (EOLAB)

Valérie Demarez (CESBIO)

David Morin (CESBIO)

<b>Project co-funded by the European Commission within the Seventh Framework Program (2007-2013)</b>		
<b>Dissemination Level</b>		
PU	Public	<b>X</b>
PP	Restricted to other programme participants (including the Commission Services)	
RE	Restricted to a group specified by the consortium (including the Commission Services)	
CO	Confidential, only for members of the consortium (including the Commission Services)	

## DOCUMENT RELEASE SHEET

<b>Book Captain:</b>	J. Sanchez	Date: 08.06.2016	Sign 
<b>Approval:</b>	R. Lacaze	Date:10.06.2016	Sign. 
<b>Endorsement:</b>	M. Koleva	Date:	Sign.
<b>Distribution:</b>	Public		

## CHANGE RECORD

Issue/Revision	Date	Page(s)	Description of Change	Release
	26.06.2014	All	First issue	I1.00
I1.10	08.10.2014	All	Included comments from CESBIO	I1.10
I1.20	08.06.2016	All	Revision of the final ImagineS database	I1.20

## TABLE OF CONTENTS

<b>1. Background of the Document</b>	<b>10</b>
1.1 Executive Summary	10
1.2 Portfolio	10
1.3 Scope and Objectives	11
1.4 Content of the Document	11
<b>2. Introduction</b>	<b>12</b>
<b>3. Study area</b>	<b>14</b>
3.1. Location	14
3.2. Description Of The Test Site	14
<b>4. Ground measurements</b>	<b>17</b>
4.1 Material and Methods	17
4.2 Spatial Sampling Scheme	18
4.3 Content of the Ground Dataset	19
<b>5. Evaluation of the sampling</b>	<b>23</b>
5.1 Principles	23
5.2 Evaluation Based On NDVI Values	23
5.3 Evaluation Based On Convex Hull: Product Quality Flag	25
<b>6. Estimation of the High Resolution Maps</b>	<b>27</b>
6.1 Imagery	27
6.2 The Transfer Function	28
6.2.1. The regression method	28
6.2.2. Band combination	28
6.2.3. The selected Transfer Function	28
6.3 The High Resolution Ground Based Maps	35
<b>7. Conclusions</b>	<b>44</b>
<b>8. Acknowledgements</b>	<b>46</b>
<b>9. References</b>	<b>47</b>
<b>ANNEX I: STATISTICS OF GROUND DATA</b>	<b>51</b>

**ANNEX II: INTERCOMPARISON OF TF RESULTS FOR THE CAMPAIGN THREE BETWEEN  
SPOT5 AND LANDSAT8..... 60**

## LIST OF FIGURES

Figure 1. Location of the SouthWest site near Toulouse in France. ....	14
Figure 2. Distribution of the sampling units in the study area (20x20km <sup>2</sup> ). The red squares show the two selected 3x3km <sup>2</sup> areas for validation. Source: Google Earth.....	15
Figure 3. View of the two selected areas for validation (5x5 km <sup>2</sup> ). Left: SW1. Right: SW2. Source: Google Earth. ....	15
Figure 4: Temporal variations of two Maize ESUs (Mais 4 and Mais 8) during the field experiment in 2013 for LAI, FAPAR and FCOVER. The rectangles define the period of the campaigns 1-5.....	20
Figure 5: Temporal variations of two Sun Flower ESUs (Tournesol2 and Tournesol5) during the field experiment in 2013 for LAI, FAPAR and FCOVER. The rectangles define the period of the campaigns 1-5. ....	21
Figure 6: Temporal variations of the measurements of two Wheat ESUs (Ble 1 and Ble 9) during the field experiment in 2013 for LAI, FAPAR and FCOVER. The rectangle defines the period of the campaign 1. ....	22
Figure 7: Comparison of NDVI TOA distribution between ESUs (green dots) and over the whole image (blue line). Top Left: First Campaign (19 <sup>th</sup> – 26 <sup>th</sup> of June, 2013). Top Right: Second Campaign (9 <sup>th</sup> – 11 <sup>th</sup> of July, 2013). Center Left: Third Campaign (24 <sup>th</sup> – 29 <sup>th</sup> of July, 2013). Center Right: Fourth Campaign (16 <sup>th</sup> – 20 <sup>th</sup> of August, 2013). Bottom: Fifth Campaign (2 <sup>th</sup> – 6 <sup>th</sup> of September, 2013).....	24
Figure 8: Convex Hull test over 20x20km <sup>2</sup> area centered at the test site: clear and dark blue correspond to the pixels belonging to the 'strict' and 'large' convex hulls and red to the pixels for which the transfer function is extrapolating. Black corresponds with no values.....	26
Figure 9: Test of multiple regression (Transfer Function) applied on different band combinations. Band combinations are given in abscissa (1=G, 2=RED, 3=NIR and 4=SWIR). The weighted root mean square error (RMSE) is presented in red along with the cross-validation RMSE in green. The numbers indicate the number of data used for the robust regression with a weight lower than 0.7 that could be considered as outliers. Top: First campaign (19 <sup>th</sup> – 26 <sup>th</sup> of June, 2013). Bottom: Second campaign (9 <sup>th</sup> – 11 <sup>th</sup> of July, 2013).....	30
Figure 10: Test of multiple regression (Transfer Function) applied on different band combinations. Band combinations are given in abscissa (1=G, 2=RED, 3=NIR and 4=SWIR). The weighted root mean square error (RMSE) is presented in red along with the cross-validation RMSE in green. The numbers indicate the number of data used for the robust regression with a weight lower than 0.7 that could be considered as outliers. Top: Third campaign (24 <sup>th</sup> – 29 <sup>th</sup> of July, 2013). Bottom: Fourth campaign (16 <sup>th</sup> – 20 <sup>th</sup> of August, 2013).....	31
Figure 11: Test of multiple regression (Transfer Function) applied on different band combinations. Band combinations are given in abscissa (1=G, 2=RED, 3=NIR and 4=SWIR). The weighted root mean square error (RMSE) is presented in red along with the cross-validation RMSE in green. The numbers indicate the number of data used for the robust regression with a weight lower than 0.7 that could be considered as outliers. Fifth campaign (2 <sup>th</sup> – 6 <sup>th</sup> of September, 2013).....	32
Figure 12: LAI <sub>eff</sub> , LAI, FAPAR and FCOVER: results for regression on reflectance using 4 bands combination. Full dots: Weight > 0.7. Empty dots: 0 < Weight < 0.7. Crosses (if any): Weight = 0. Top: First campaign (19 <sup>th</sup> – 26 <sup>th</sup> of June, 2013). Bottom: Second campaign (9 <sup>th</sup> – 11 <sup>th</sup> of July, 2013) .....	33
Figure 13: LAI <sub>eff</sub> , LAI, FAPAR and FCOVER: results for regression on reflectance using 4 bands combination. Full dots: Weight > 0.7. Empty dots: 0 < Weight < 0.7. Crosses (if any): Weight = 0. Top: Third campaign (24 <sup>th</sup> – 29 <sup>th</sup> of July, 2013). Bottom: Fourth campaign (16 <sup>th</sup> – 20 <sup>th</sup> of August, 2013).....	34
Figure 14: LAI <sub>eff</sub> , LAI, FAPAR and FCOVER: results for regression on reflectance using 4 bands combination. Full dots: Weight > 0.7. Empty dots: 0 < Weight < 0.7. Crosses (if any): Weight = 0. Fifth campaign (2 <sup>th</sup> – 6 <sup>th</sup> of September, 2013). ....	35
Figure 15: Ground-based biophysical LAI maps applied on the 5x5 km <sup>2</sup> SW1 area for all the Campaigns. Second and Third campaign are based on SPOT-5, the others on LANDSAT-8.....	36

*Figure 16: Ground-based biophysical FAPAR maps applied on the 5x5 km<sup>2</sup> SW1 area for all the Campaigns. Second and Third campaign are based on SPOT-5, the others on LANDSAT-8. .... 37*

*Figure 17: Ground-based biophysical LAI maps applied on the 5x5 km<sup>2</sup> SW2 area for all the Campaigns. Second and Third campaign are based on SPOT-5, the others on LANDSAT-8. .... 38*

*Figure 18: HR biophysical FAPAR maps applied on the 5x5 km<sup>2</sup> SW2 area for all the Campaigns. Second and Third campaign are based on SPOT-5, the others on LANDSAT-8. .... 39*

*Figure 19: Temporal variations of the mean values over SW1 3x3km<sup>2</sup> area for LAI<sub>eff</sub>, LAI, FAPAR and FCOVER.. 41*

*Figure 20: Temporal variations of the mean values over SW2 3x3km<sup>2</sup> area for LAI<sub>eff</sub>, LAI, FAPAR and FCOVER.. 42*



## LIST OF TABLES

---

<i>Table 1: Ground Campaign and SPOT5 Imagery available.....</i>	<i>13</i>
<i>Table 2: Coordinates and altitude of the test site. ....</i>	<i>16</i>
<i>Table 3: Summary of the field measurements in SouthWest site.....</i>	<i>19</i>
<i>Table 4: The File template used to describe ESUs with the ground measurements.....</i>	<i>19</i>
<i>Table 5: Acquisition geometry of SPOT5 HRG 2 data used for retrieving high resolution maps.....</i>	<i>27</i>
<i>Table 6: Acquisition geometry of LANDSAT8 data used for retrieving high resolution maps. ....</i>	<i>27</i>
<i>Table 7: Transfer function applied to the whole site for LA<sub>eff</sub>, LAI and FAPAR. RW for weighted RMSE, and RC for cross-validation RMSE. ....</i>	<i>29</i>
<i>Table 8: Mean values and standard deviation (STD) of the HR biophysical maps for the 3x3km<sup>2</sup> SouthWest site 1.....</i>	<i>40</i>
<i>Table 9: Mean values and standard deviation (STD) of the HR biophysical maps for the 3x3km<sup>2</sup> SouthWest site 2.....</i>	<i>40</i>
<i>Table 10: Content of the dataset.....</i>	<i>43</i>

## 1. BACKGROUND OF THE DOCUMENT

### 1.1 EXECUTIVE SUMMARY

The Copernicus Land Service has been built in the framework of the FP7 geoland2 project, which has set up pre-operational infrastructures. ImagineS intends to ensure the continuity of the innovation and development activities of geoland2 to support the operations of the global land component of the GMES Initial Operation (GIO) phase. In particular, the use of the future Sentinel data in an operational context will be prepared. Moreover, IMAGINES will favor the emergence of new downstream activities dedicated to the monitoring of crop and fodder production.

The main objectives of ImagineS are to (i) improve the retrieval of basic biophysical variables, mainly LAI, FAPAR and the surface albedo, identified as Terrestrial Essential Climate Variables, by merging the information coming from different sensors (PROBA-V and Landsat-8) in view to prepare the use of Sentinel missions data; (ii) develop qualified software able to process multi-sensor data at the global scale on a fully automatic basis; (iii) complement and contribute to the existing or future agricultural services by providing new data streams relying upon an original method to assess the above-ground biomass, based on the assimilation of satellite products in a Land Data Assimilation System (LDAS) in order to monitor the crop/fodder biomass production together with the carbon and water fluxes; (iv) demonstrate the added value of this contribution for a community of users acting at global, European, national, and regional scales.

Further, ImagineS serves the growing needs of international (e.g. FAO and NGOs), European (e.g. DG AGRI, EUROSTATS, DG RELEX), and national users (e.g. national services in agro-meteorology, ministries, group of producers, traders) on accurate and reliable information for the implementation of the EU Common Agricultural Policy, of the food security policy, for early warning systems, and trading issues. ImagineS will also contribute to the Global Agricultural Geo-Monitoring Initiative (GEO-GLAM) by its original agriculture service which can monitor crop and fodder production together with the carbon and water fluxes and can provide drought indicators, and through links with JECAM (Joint Experiment for Crop Assessment and Monitoring).

### 1.2 PORTFOLIO

The ImagineS portfolio contains global and regional biophysical variables derived from multi-sensor satellite data, at different spatial resolutions, together with agricultural indicators, including the above-ground biomass, the carbon and water fluxes, and drought indices resulting from the assimilation of the biophysical variables in the Land Data Assimilation System (LDAS).

The production in Near Real Time of the 333m resolution products, at a frequency of 10 days, using PROBA-V data is carried out in the Copernicus Global Land Service (<http://land.copernicus.eu/global/>).

The demonstration of high resolution (30m) products derived from Landsat-8 was done over demonstration sites of cropland and grassland in contrasting climatic and environmental conditions. Demonstration products are available on the ImagineS website (<http://www.fp7-imagines.eu/pages/services-and-products/landsat-8-biophysical-products.php>)

### 1.3 SCOPE AND OBJECTIVES

The main objective of this document is to describe the ground database provided by CESBIO, and the processing carried out by EOLAB to derive the high resolution biophysical maps. These maps correspond to the map derived from the determination of a transfer function between reflectance values of TOA SPOT5 and LANDSAT8 images acquired around the ground campaign, and biophysical variable measurements (hemispherical images). The derived biophysical variable maps are:

- Leaf Area Index: Two LAI maps are produced per campaign, the first one corresponds to effective LAI (LAI<sub>eff</sub>) derived from the description of the gap fraction as a function of the view zenith angle, and the second one (LAI) corresponds to the 'actual' LAI, which is derived from the LAI<sub>eff</sub> and the clumping factor. Leaf Area Index refers to green elements (GAI).
- Fraction of Absorbed Photosynthetically Active Radiation (FAPAR): It is the fraction of the Photosynthetically active radiation (PAR=400-700nm) absorbed by a vegetation canopy. PAR is the solar radiation reaching the canopy in the 0.4–0.7  $\mu\text{m}$  wavelength region. We focused on the daily integrated FAPAR computed as the black-sky FAPAR integrated over the day. In addition, two other quantities are provided: the instantaneous 'black-sky' FAPAR at 10:00h, which is the FAPAR under direct illumination conditions at a given solar position and the 'white-sky' FAPAR, which is the FAPAR under diffuse illumination conditions.
- Fraction of green Vegetation Cover (FCOVER), defined as the proportion of soil covered by vegetation, derived from the gap fraction between 0 and 10° of view zenith angle.

### 1.4 CONTENT OF THE DOCUMENT

This document is structured as follows:

- Chapter 2 provides an introduction to the field experiment.
- Chapter 3 provides the location and description of the site.
- Chapter 4 describes the ground measurements, including material and methods, sampling and data processing.
- Chapter 5 describes an evaluation of the sampling.
- Chapter 6 describes the methodology to derive high resolution maps of the biophysical variables using a transfer function, and results.

## 2. INTRODUCTION

Validation of remote sensing products is mandatory to guaranty that the satellite products meets the user's requirements. Protocols for validation of global LAI products are already developed in the context of Land Product Validation (LPV) group of the Committee on Earth Observation Satellite (CEOS) for the validation of satellite-derived land products (Fernandes et al., 2012), and recently applied to Copernicus global land products based on SPOT/VGT observation (Camacho et al., 2013). This generic approach is made of 2 major components:

- The indirect validation: including inter-comparison between products as well as evaluation of their temporal and spatial consistency
- The direct validation: comparing satellite products to ground measurements of the corresponding biophysical variables. In the case of low and medium resolution sensors, the main difficulty relies on scaling local ground measurements to the extent corresponding to pixels size. However, the direct validation is limited by the small number of sites, for that reason a main objective of ImagineS is the collection of ground truth data in demonstration sites.

The content of this document is compliant with existing validation guidelines (the generation for up-scaling ground maps for direct validation) as proposed by the CEOS LPV group (Morissette et al., 2006); the VALERI project (<http://w3.avignon.inra.fr/valeri/>) and ESA campaigns (Baret and Fernandes, 2012). It therefore follows the general strategy based on a bottom up approach: it starts from the scale of the individual measurements that are aggregated over an elementary sampling unit (ESU) corresponding to a support area consistent with that of the high resolution imagery used for the up-scaling of ground data. Several ESUs are sampled over the site. Radiometric values over a decametric image are also extracted over the ESUs. This will be later used to develop empirical transfer functions for up-scaling the ESU ground measurements (e.g. Martínez et al., 2009). Finally, the high resolution ground based map will be compared with the medium resolution satellite product at the spatial support of the product.

A multi-temporal campaign to characterize the biophysical parameters of different crop types at the SouthWest test site during spring and summer of 2013 was carried out and provided by CESBIO. EOLAB has grouped these multi-temporal data on five periods ("campaigns", see Table 1). The five campaigns were selected to increase the number of ground points for up-scaling but considering periods lower than a week in order to group consistent vegetation measurements. Ground data acquired before 19<sup>th</sup> of June was not used here due to the low number of ESUs available. Table 1 describes the period of the field data acquisition for each campaign, and the imagery available in order to apply the Transfer Function. Two SPOT5 images over SouthWest test site are provided by the GSCDA (GMES Space Component Data Access). The other three LANDSAT8 images are downloaded through the USGS Global Visualization Viewer service (<http://glovis.usgs.gov/AboutBrowse.shtml#landsatarchivedescription>).

**Table 1: Ground Campaign and SPOT5 and LANDSAT8 Imagery available.**

<b>CAMPAIGN</b>	<b>DATES</b>	<b>IMAGERY</b>
<b>First campaign</b>	19 <sup>th</sup> to 26 <sup>th</sup> of June 2013	LANDSAT8 TOA (26.06.2013)
<b>Second campaign</b>	9 <sup>th</sup> to 11 <sup>th</sup> of July 2013.	SPOT5 TOA (15.07.2013)
<b>Third campaign</b>	24 <sup>th</sup> to 29 <sup>th</sup> of July 2013	SPOT5 TOA (25.07.2013)
<b>Fourth campaign</b>	16 <sup>th</sup> to 20 <sup>th</sup> of August 2013	LANDSAT8 TOA (20.08.2013)
<b>Fifth campaign</b>	2 <sup>nd</sup> to 6 <sup>th</sup> of September	LANDSAT8 TOA (29.08.2013)

**Team involved in field collection:**

Dr. Valerie Demarez and David Morin (CESBIO)

Contact: valerie.demarez@cesbio.cnes.fr

## 3. STUDY AREA

### 3.1. LOCATION

The experimental site is located near Toulouse, in the Southwest of France. The central coordinate of the study area, near the Garonne River is 43.504° N, 1.171° E.

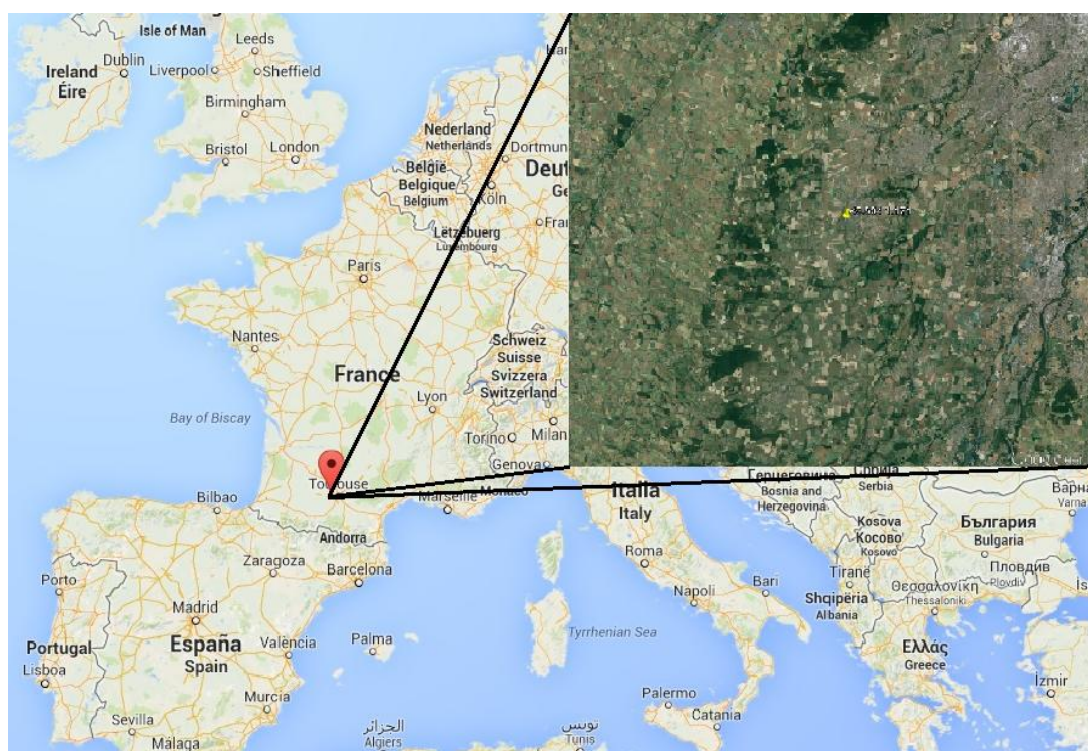


Figure 1. Location of the SouthWest site near Toulouse in France.

### 3.2. DESCRIPTION OF THE TEST SITE

Croplands cover about 50% of the selected study area. The remaining 50% corresponds to urban area (city of Toulouse in the north-east), forest, natural vegetation, and water bodies. The southeastern and the western parts of the study area are hilly landscapes with small fields (approximately 10 ha) and covered by non-irrigated crops (mainly wheat, rapeseed and sunflower). The study area is generally flat with large fields (approximately 25 ha) and covered by a mix of irrigated (mainly maize and soybean) and non-irrigated crops (mainly sunflower, wheat and rapeseed) (Claverie et al., 2013).

Figure 2 shows the distribution of the ESUs along the 20x20 km<sup>2</sup> region around the central coordinate. Two homogeneous cropland areas of 3x3 km<sup>2</sup> are chosen for the direct validation of the satellite product. These 3x3 km<sup>2</sup> areas (see red squares in figure 2) have been chosen at the west of the central coordinate (SW1) and at the south of the central coordinate (SW2),



covering crops and avoiding urban areas or water bodies. The validation areas have been selected to have two different temporal variations (spring crops and summer crops). Figure 3 shows the 3x3km<sup>2</sup> areas of the two selected validation regions (5x5 km<sup>2</sup>). Mean values of the biophysical parameter are computed over 3x3 km<sup>2</sup> while maps are provided over 5x5 km<sup>2</sup>.

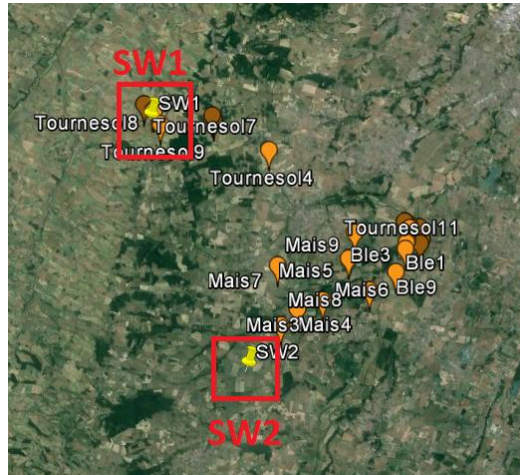


**Figure 2. Distribution of the sampling units in the study area (20x20km<sup>2</sup>).The red squares show the two selected 3x3km<sup>2</sup> areas for validation. Source: Google Earth**

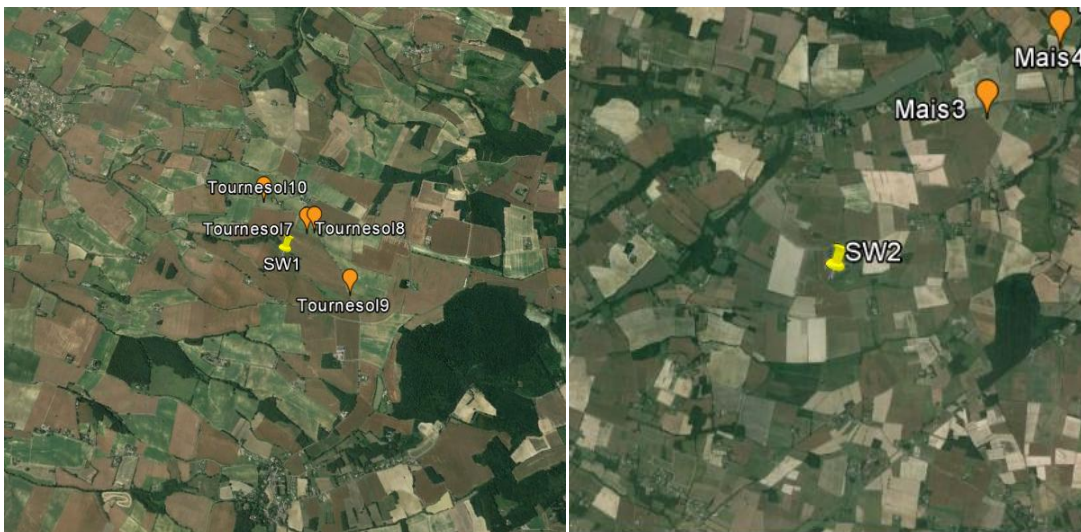


**Figure 3.View of the two selected areas for validation (5x5 km<sup>2</sup>). Left: SW1. Right: SW2. Source: Google Earth.**

**Table 2: Coordinates and altitude of the test site.**

20x20 km <sup>2</sup> Center Site		
Geographic Lat/lon, WGS-84 (degrees)	Latitude=43.504° N Longitude=1.171° E	
Altitude	219 m	
3x3 km <sup>2</sup> CenterSites	SW1	SW2
Geographic Lat/lon, WGS-84 (degrees)	Latitude=43.5511111° N Longitude=1.088889° E	Latitude=43.44708° N Longitude=1.14505° E
Altitude	231 m	236 m



## 4. GROUND MEASUREMENTS

### 4.1 MATERIAL AND METHODS

**Digital Hemispheric Photographs (DHP)** were acquired with a Digital hemispherical camera. Hemispherical photos allow the calculation of LAI measuring gap fraction through an extreme wide-angle camera lens (i.e. 180°) (Weiss et al., 2004). It produces circular images that record the size, shape, and location of gaps, either looking upward from within a canopy or looking downward from above the canopy.

The hemispherical images acquired during the field campaigns are processed with the Can-Eye software (<http://www6.paca.inra.fr/can-eye>) to derive Effective LAI (LAI<sub>eff</sub>), LAI, FAPAR and FCOVER. It is based on a RGB colour classification of the image to discriminate vegetation elements from background (i.e., gaps). This approach allows exploiting downward-looking photographs for short canopies (background = soil) as well as upward-looking photographs for tall canopies (background = sky). Can-Eye software processes simultaneously up to N = 25 images acquired over the same ESU. Note that the N images were acquired with similar illumination conditions to limit the variation of colour dynamics between images.

The CAN-EYE software computes biophysical variables from gap fraction as follows:

**Effective LAI (LAI<sub>eff</sub>)** is computed from the gap fraction  $P_0$  following the Poisson law (Welles and Norman, 1991):

$$P_0(\theta_v, \varphi_v) = e^{-G \cdot (\theta_v, \varphi_v) \frac{LAI_{eff}}{\cos(\theta_v)}} \quad \text{Eq. (1)}$$

where  $\theta$  and  $\varphi$  are respectively the zenith and azimuth angles of the direction of propagation of the incident beam, LAI<sub>eff</sub> refers to effective LAI, G is the mean projection of a leaf area unit in a plane perpendicular to direction  $(\theta, \varphi)$  which is directly dependent of the leaf angle distribution (LAD). LAD is assumed to be uniform in azimuth and following an ellipsoidal distribution for the inclination. It is thus fully characterized with the average leaf angle (ALA) only. Two variables are therefore needed to describe canopy architecture under these assumptions: the effective LAI (LAI<sub>eff</sub>) and effective ALA ( $\theta_{leaf,eff}$ ). A look-up-table (LUT) is used to estimate LAI<sub>eff</sub> and  $\theta_{leaf,eff}$  from the measured zenithal variation of the gap fraction (Weiss et al., 2004).

Actual LAI that can be measured only using a planimeter with however possible allometric relationships to reduce the sampling are related to the effective leaf area index through:

$$LAI_{eff} = \lambda_0 \cdot LAI \quad \text{Eq. (2)}$$

where  $\lambda_0$  is the clumping index. In CAN-EYE, the clumping index is computed using the Lang and Xiang (1986) logarithm gap fraction averaging method, although some uncertainties are associated to this method (Demarez et al., 2008). The principle is based on the assumption

that vegetation elements are locally assumed randomly distributed. Values of clumping index given by CAN\_EYE are in certain cases correlated with the size of the cells used to divide photographs.

*As the CAN-EYE software provides different results (CEV6.1, CEV5.1) for LAI and LAI<sub>eff</sub> variables, an average LAI value was provided as ground estimate, and the standard deviation of the different method LAI estimates was reported as the uncertainty of the estimate.*

**FCOVER**, is retrieved from gap fraction between 0 to 10°.

$$FCOVER = 1 - P_0 \cdot (0 - 10^\circ) \quad \text{Eq. (3)}$$

**FAPAR**. As there is little scattering by leaves in that particular spectral domain due to the strong absorbing features of the photosynthetic pigments, FAPAR is often assumed to be equal to FIPAR (Fraction of Intercepted Photosynthetically Active Radiation), and therefore to the gap fraction. The actual FAPAR is the sum of two terms, weighted by the diffuse fraction in the PAR domain: the 'black sky' FAPAR that corresponds to the direct component and the 'white sky' or the diffuse component.

The instantaneous "Black-sky FAPAR" ( $FAPAR^{BS}$ ) is given at a solar position (date, hour and latitude). Depending on latitude, the CAN EYE computes the solar zenith angle every solar hour during half the day (there is symmetry at 12:00). The instantaneous FAPAR is then approximated at each solar hour as the gap fraction in the corresponding solar zenith angle:

$$FAPAR^{BS}(\theta_S) = 1 - P_0 \cdot (\theta_S) \quad \text{Eq. (4)}$$

The daily integrated black sky or direct FAPAR is computed as the following:

$$FAPAR_{Day}^{BS} = \frac{\int_{sunset}^{sunrise} \cos(\theta_S) \cdot [1 - P_0 \cdot (\theta_S)] \cdot d\theta}{\int_{sunset}^{sunrise} \cos(\theta_S) \cdot d\theta} \quad \text{Eq. (5)}$$

## 4.2 SPATIAL SAMPLING SCHEME

A total of 23, 18, 20, 19 and 18 ESUs were characterized during the first, second, third, fourth and fifth campaigns respectively over three different cropland types. Furthermore, 3 soil ESUs have been added in order to extend the sampling over non vegetated areas. A pseudo-regular sampling was used within each ESU of approximately 20x20 m<sup>2</sup>. The centre of the ESU was geo-located using a GPS. The number of hemispherical photos per ESU ranges between 12 and 15.

Table 3 summarizes the number of sampling units (ESUs) per each crop type acquired during the "five" field campaigns. Note that three additional Soil ESUs were added.

**Table 3: Summary of the field measurements in SouthWest site.**

Land Use	Number of ESU's				
	First Campaign (19 <sup>th</sup> – 26 <sup>th</sup> of June, 2013)	Second Campaign (9 <sup>th</sup> – 11 <sup>th</sup> of July, 2013)	Third Campaign (24 <sup>th</sup> - 29 <sup>th</sup> of July, 2013)	Fourth Campaign (16 <sup>th</sup> - 20 <sup>th</sup> of August, 2013)	Fifth Campaign (2 <sup>th</sup> – 6 <sup>th</sup> of September, 2013)
Sunflower (T)	10	9	11	11	11
Maize (M)	8	9	9	8	7
Wheat (B)	5	0	0	0	0
Soil	3	3	3	3	3
<b>TOTAL</b>	<b>26</b>	<b>21</b>	<b>23</b>	<b>22</b>	<b>21</b>

### 4.3 CONTENT OF THE GROUND DATASET

Each ESU is described according to an agreed format. For this purpose a template file has been used (Table 4).

**Table 4: The File template used to describe ESUs with the ground measurements.**

Column	Var.Name	Comment	
1	Plot #	Number of the field plot in the site	
2	Plot Label	Label of the plot in the site	
3	ESU #	Number of the Elementary Sampling Unit (ESU)	
4	ESU Label	Label of the ESU in the campaign	
5	Northing Coord.	Geographical coordinate: Latitude (°), WGS-84	
6	Easting Coord.	Geographical coordinate: Longitude (°), WGS-84	
7	Extent (m) of ESU (diameter)	Size of the ESU <sup>(1)</sup>	
8	Land Cover	Detailed land cover	
9	Start Date (dd/mm/yyyy)	Starting date of measurements	
10	End Date (dd/mm/yyyy)	Ending date of measurements	
11+4*j (*)	LAI	Method	Instrument
12+4*j (*)		Nb. Replications	Number of Replications
13+4*j (*)		PRODUCT	Methodology
14+4*j (*)		Uncertainty	Standard deviation

(\*)j=0:3. For LAI, LAI<sub>eff</sub>, FAPAR and FCOVER.

The bar graphs of the measures per different field plot and the histograms of each campaign are provided in ANNEX I.

Figure 4 shows the typically temporal variation over 2 ESUs of Maize (Mais4 and Mais8) during the field experiment for LAI, FAPAR and FCOVER. Distribution of LAI values range between 0 to 4, between 0 and 0.9 for FAPAR and between 0 and 0.7 for FCOVER. LAI

behavior shows an increase of the value up to campaign 4 (mid-August), with a slight decrease during the campaign5 (beginning of September). FAPAR measures behave consistently, but FCOVER maximum values are obtained in campaign 5 or after (Mais4).

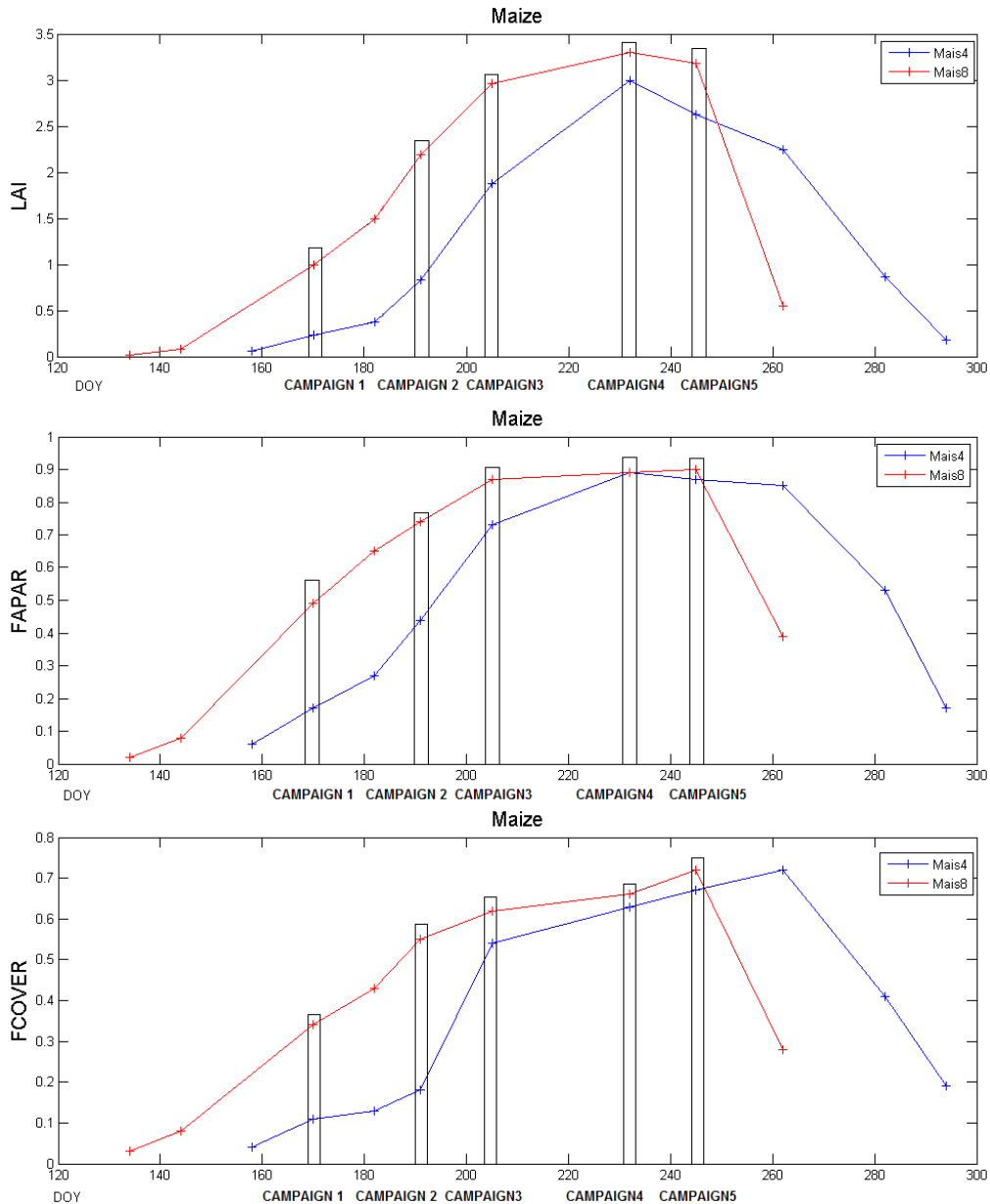


**Figure 4: Temporal variations of two Maize ESUs (Mais 4 and Mais 8) during the field experiment in 2013 for LAI, FAPAR and FCOVER. The rectangles define the period of the campaigns1-5.**

Figure 5 shows the temporal variations over two sunflower ESUs (Tournesol 2 and Tournesol 5). Distribution of LAI values range between 0 to 1.9, between 0 and 0.8 for

FAPAR and between 0 and 0.7 for FCOVER. LAI, FAPAR and FCOVER behavior shows an increase of the value during campaigns 1 (mid-June) and 2 (beginning of July), maximum value around DOY 200 (July 19<sup>th</sup>) and after the senescent period with decreasing LAI and FAPAR values (campaigns 3, 4, 5).

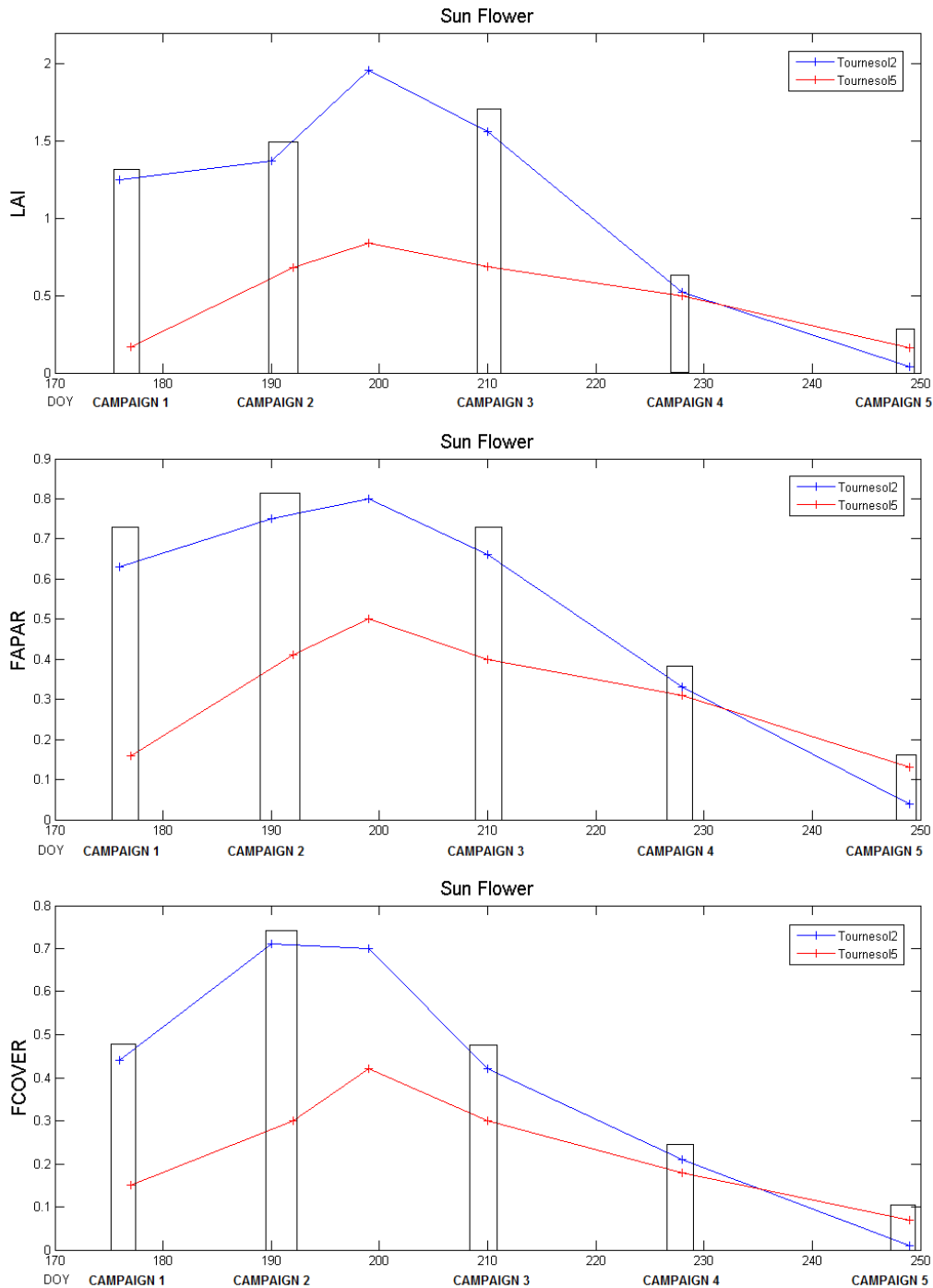


**Figure 5: Temporal variations of two Sun Flower ESUs (Tournesol2 and Tournesol5) during the field experiment in 2013 for LAI, FAPAR and FCOVER. The rectangles define the period of the campaigns1-5.**

Figure 6 shows the temporal variations over the two wheat ESUs (Ble 1 and Ble 9). Wheat measurements were coincident with maize only for the first campaign. These measures of wheat correspond to a spring crop type, reaching senescent state at the end of June (i.e. after campaign 1), while maize and sunflower are summer crops, starting at the end of the wheat cycle.

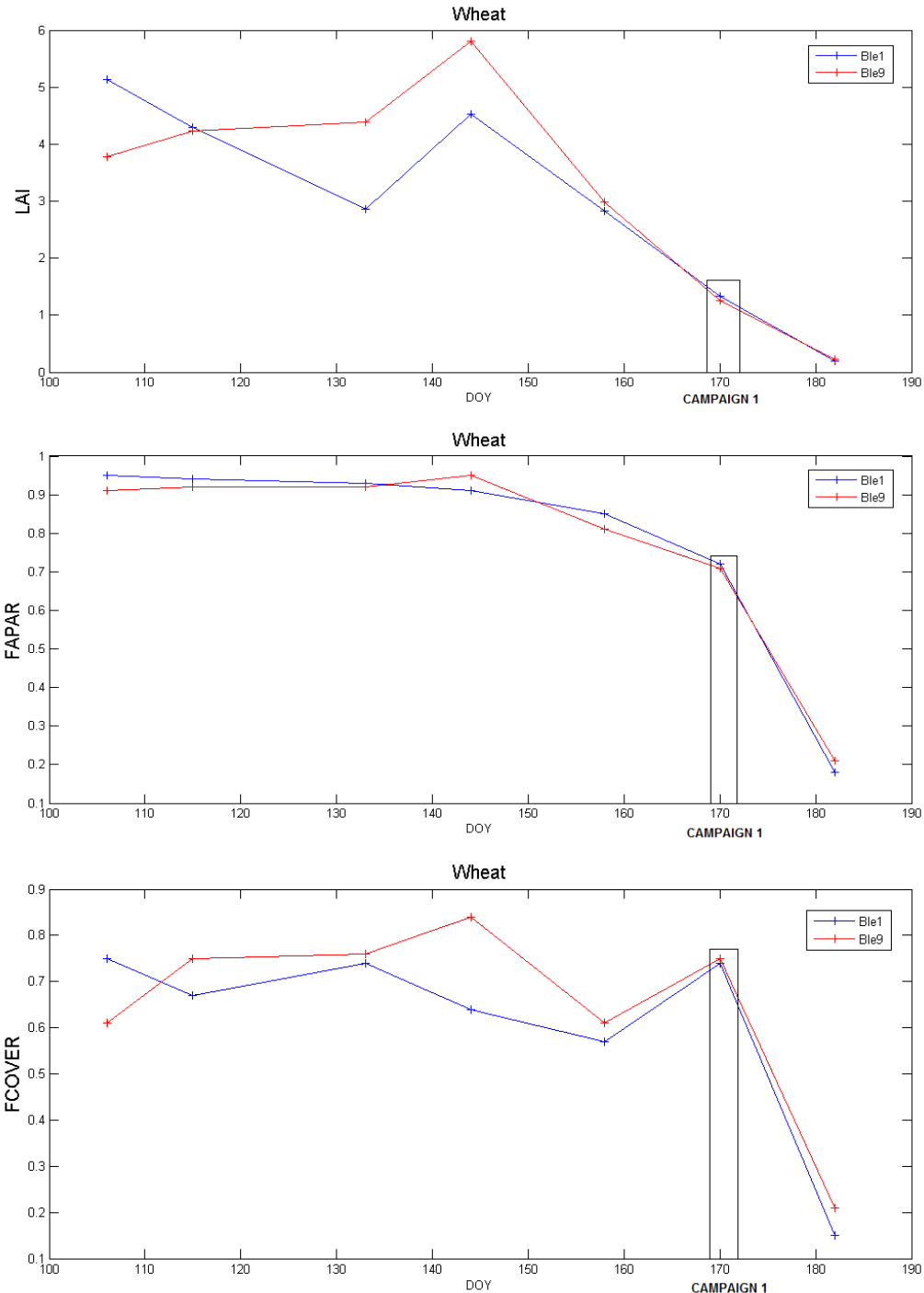


**Figure 6: Temporal variations of the measurements of two Wheat ESUs (Ble 1 and Ble 9) during the field experiment in 2013 for LAI, FAPAR and FCOVER. The rectangle defines the period of the campaign 1.**

## 5. EVALUATION OF THE SAMPLING

### 5.1 PRINCIPLES

Based on previous field activities, the data set sampling was concentrated in the most representative crops. The number of ESUs was of 26, 21, 23,22 and 21 for the five campaigns respectively.

### 5.2 EVALUATION BASED ON NDVI VALUES

The sampling strategy is evaluated using the SPOT5 or LANDSAT8 image by comparing the NDVI distribution over the site with the NDVI distribution over the ESUs (Figure 7). As the number of pixels is drastically different for the ESU and whole site (WS) it is not statistically consistent to directly compare the two NDVI histograms. Therefore, the proposed technique consists in comparing the NDVI cumulative frequency of the two distributions by a Monte-Carlo procedure which aims at comparing the actual frequency to randomly shifted sampling patterns. It consists in:

1. computing the cumulative frequency of the  $N$  pixel NDVI that correspond to the exact ESU locations; then, applying a unique random translation to the sampling design (modulo the size of the image)
2. computing the cumulative frequency of NDVI on the randomly shifted sampling design
3. repeating steps 1 and 2, 199 times with 199 different random translation vectors.

This provides a total population of  $N = 199 + 1$ (actual) cumulative frequency on which a statistical test at acceptance probability  $1 - \alpha = 95\%$  is applied: for a given NDVI level, if the actual ESU density function is between two limits defined by the  $N\alpha/2 = 5$  highest and lowest values of the 200 cumulative frequencies, the hypothesis assuming that WS and ESU NDVI distributions are equivalent is accepted, otherwise it is rejected.

Figure 7 shows the NDVI TOA distribution of the five campaigns. The NDVI TOA distribution is good over the whole site (comprised between the 5 highest and lowest cumulative frequencies) for the campaigns 1, 2, 3, 4 and 5.

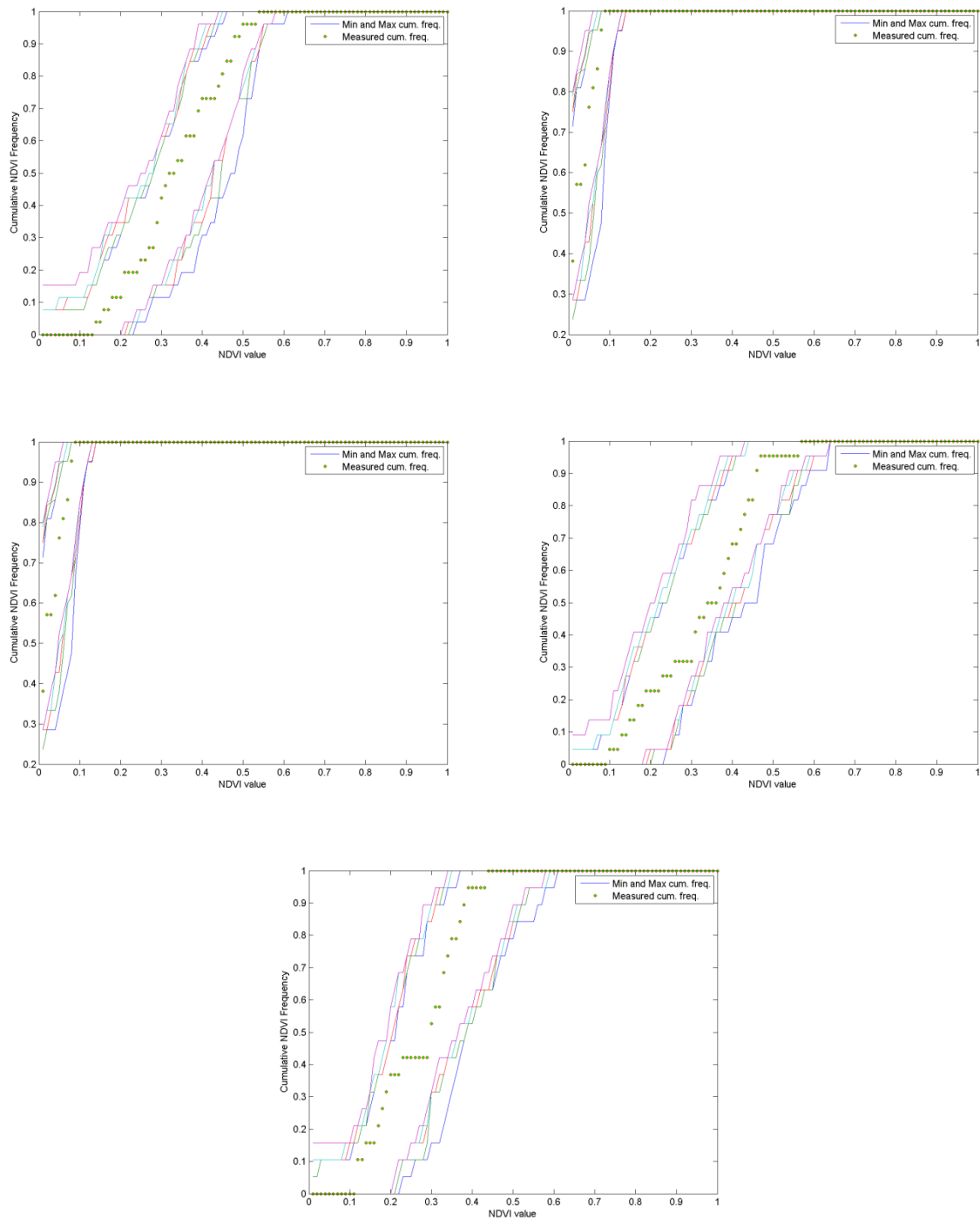


**Figure 7: Comparison of NDVI TOA distribution between ESUs (green dots) and over the whole image (blue line). Top Left: First Campaign (19<sup>th</sup>– 26<sup>th</sup> of June, 2013). Top Right: Second Campaign (9<sup>th</sup>– 11<sup>th</sup> of July, 2013). Center Left: Third Campaign (24<sup>th</sup>- 29<sup>th</sup> of July, 2013). Center Right: Fourth Campaign (16<sup>th</sup>- 20<sup>th</sup> of August, 2013). Bottom: Fifth Campaign (2<sup>th</sup>- 6<sup>th</sup> of September, 2013).**



### 5.3 EVALUATION BASED ON CONVEX HULL: PRODUCT QUALITY FLAG.

The interpolation capabilities of the empirical transfer function used for up-scaling the ground data using decametric images is dependent of the sampling (Martinez et al., 2009). A test based on the convex hulls was also carried out to characterize the representativeness of ESUs and the reliability of the empirical transfer function using the four selected bands (green, red, NIR and SWIR) of the SPOT5 and LANDSAT8 images. Flag images are computed over the reflectances. The result on convex-hulls can be interpreted as:

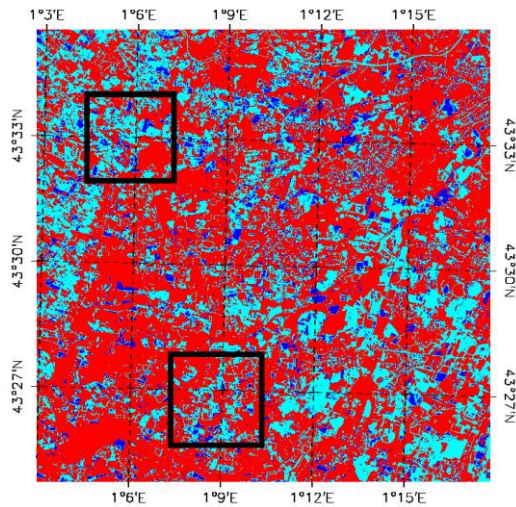
- pixels inside the 'strict convex-hull': a convex-hull is computed using all the SPOT5 or Landsat-8 reflectances corresponding to the ESUs belonging to each vegetation class. These pixels are well represented by the ground sampling and therefore, when applying a transfer function the degree of confidence in the results will be quite high, since the transfer function will be used as an interpolator;
- pixels inside the 'large convex-hull': a convex-hull is computed using all the reflectance combinations up to  $\pm 5\%$  in relative value corresponding to the ESUs. For these pixels, the degree of confidence in the obtained results will be quite good, since the transfer function is used as an extrapolator (but not far from interpolator);
- pixels outside the two convex-hulls: this means that for these pixels, the transfer function will behave as an extrapolator which makes the results less reliable. However, having a priori information on the site may help to evaluate the extrapolation capacities of the transfer function.

Figure 8 shows the results of the Convex-Hull test (i.e., Quality Flag images) for the SouthWest site over a  $20 \times 20 \text{ km}^2$  area where all the ground data are located. The two black squares in each image show the two selected  $3 \times 3 \text{ km}^2$  validation areas.

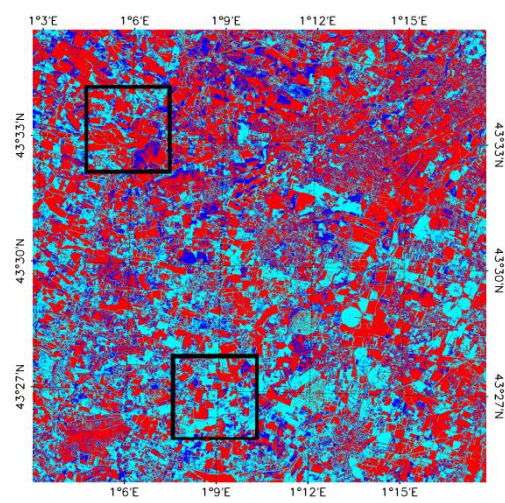
As expected due to the low number of crop types sampled (3) and the heterogeneity of the large area ( $20 \times 20 \text{ km}^2$ ) the QF shows low percentage of values inside the strict and large convex-hulls (i.e., TF behaves as interpolator). The values range between 25% (fifth campaign) and 51% (second campaign). Therefore, the resulting maps over the extended area should be considered carefully using the QF information. For the selected validation regions ( $3 \times 3 \text{ km}^2$ ), the results are slightly better, typically 45%. A further analysis of the consistency of values will be checked over the crop areas where the QF behaves as extrapolator.

Note that the image of the fifth campaign has around 5% of cloud pixels that have been filtered using the Quality Flag of the LANDSAT8 image (see black areas, no values).

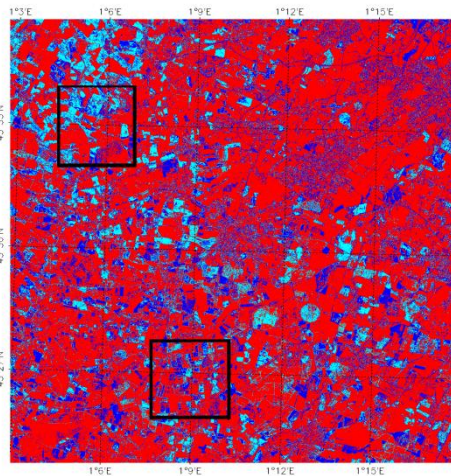
**First Campaign(19<sup>th</sup>– 26<sup>th</sup> of June, 2013)**



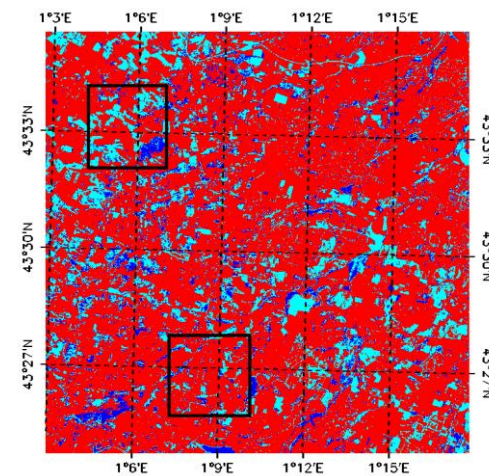
**Second Campaign(9<sup>th</sup>– 11<sup>th</sup> of July, 2013)**



**Third Campaign(24<sup>th</sup>- 29<sup>th</sup> of July, 2013)**



**Fourth Campaign(16<sup>th</sup>- 20<sup>th</sup> of August, 2013)**



**Fifth Campaign(2<sup>th</sup>- 6<sup>th</sup> of September, 2013)**

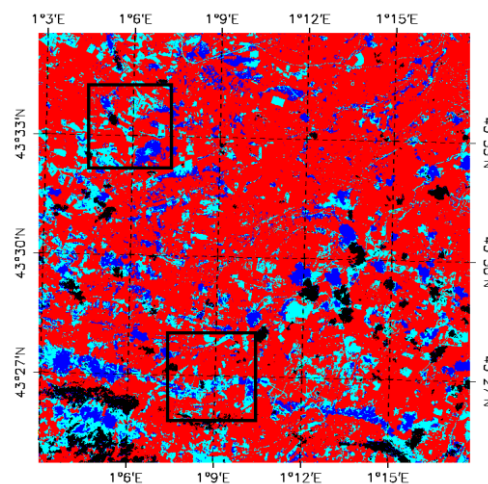


**Figure 8: Convex Hull test over 20x20km<sup>2</sup> area centered at the test site: clear and dark blue correspond to the pixels belonging to the 'strict' and 'large' convex hulls and red to the pixels for which the transfer function is extrapolating. Black corresponds with no values.**

## 6. ESTIMATION OF THE HIGH RESOLUTION MAPS

### 6.1 IMAGERY

Two SPOT5 images were acquired the 15<sup>th</sup> and 25<sup>th</sup> July 2013 (see Table 5 for acquisition geometry). These images correspond to 4 TOA reflectance spectral bands from 500nm to 1750 nm with a nadir ground sampling distance of 10 m. In order to complete the other campaigns, three LANDSAT8 images have been acquired on the dates 26<sup>th</sup> June, 20<sup>th</sup> August and 29<sup>th</sup> August 2013 (see Table 6). Four LANDSAT8 spectral bands of TOA reflectance were used from 500nm to 1650 nm with a nadir ground sampling distance of 30 m. The projection of all images is UTM 31 North, WGS84, and no atmospheric correction was applied to the images. However, as the SPOT5 and LANDSAT8 TOA reflectance images are used to compute empirical relationships between reflectance and biophysical variable, we assume that the effect of the atmosphere is the same over the whole site.

**Table 5: Acquisition geometry of SPOT5 HRG 2 data used for retrieving high resolution maps.**

SPOT 5 METADATA		
Platform / Instrument	SP05 / HRG J3	
Sensor	OPTICAL 10 m	
Spectral Range	B1(green) : 0.5-0.59 $\mu\text{m}$ B2(red) : 0.61-0.68 $\mu\text{m}$ B3(NIR) : 0.78-0.89 $\mu\text{m}$ B4(SWIR) : 1.58-1.75 $\mu\text{m}$	
	<b>Second Campaign</b> (9 <sup>th</sup> - 11 <sup>th</sup> of July, 2013)	<b>Third Campaign</b> (24 <sup>th</sup> - 29 <sup>th</sup> of July, 2013)
Acquisition date	2013-07-15	2013-07-25
Incidence angle	-11.0578°	23.1416°
Illumination Azimuth angle	129.8160°	145.8000°
Illumination Elevation angle	60.5684°	57.2000°

**Table 6: Acquisition geometry of LANDSAT8 data used for retrieving high resolution maps.**

LANDSAT8 METADATA			
Platform / Instrument	LANDSAT_8 / OLI_TIRS		
Sensor	OPTICAL 30 m		
Spectral Range	B3(green) : 0.53-0.59 $\mu\text{m}$ B4(red) : 0.64-0.67 $\mu\text{m}$ B5(NIR) : 0.85-0.88 $\mu\text{m}$ B6(SWIR1) : 1.58-1.65 $\mu\text{m}$		
	<b>First Campaign</b> (19 <sup>th</sup> - 26 <sup>th</sup> of June, 2013)	<b>Fourth Campaign</b> (16 <sup>th</sup> - 20 <sup>th</sup> of August, 2013)	<b>Fifth Campaign</b> (2 <sup>th</sup> - 6 <sup>th</sup> of September, 2013)
Acquisition date	2013-06-26	2013-08-20	2013-08-29
Illumination Azimuth angle	134.63	145.35	148.41
Illumination Elevation angle	64.65	54.99	52.4



## 6.2 THE TRANSFER FUNCTION

### 6.2.1. The regression method

If the number of ESUs is enough, multiple robust regression 'REG' between ESUs reflectance and the considered biophysical variable can be applied (Martínez et al., 2009): we used the 'robustfit' function from the Matlab statistics toolbox. It uses an iteratively re-weighted least squares algorithm, with the weights at each iteration computed by applying the bi-square function to the residuals from the previous iteration. This algorithm provides lower weight to ESUs that do not fit well. The results are less sensitive to outliers in the data as compared with ordinary least squares regression. At the end of the processing, two errors are computed: weighted RMSE (using the weights attributed to each ESU) and cross-validation RMSE (leave-one-out method). As the method has limited extrapolation capacities, a flag image (Figure 8), based on the convex hulls, is included in the final ground based map in order to inform the users on the reliability of the estimates.

### 6.2.2. Band combination

Figures 9, 10, and 11 show the results obtained for all the possible band combinations using the reflectance. The results are thus selected for LAI<sub>eff</sub>, LAI, FAPAR and FCOVER. Attending specifications of minimal noise and maximal sensitivity it has been chosen band 1 (green), band 2 (red), band 3 (Near Infrared) and band 4 (Short Wave Infrared). Note that the combination of (1, 2, 3, 4) = (G,R,NIR,SWIR) is selected for all the parameters and all campaigns.

These combinations on reflectance were selected since they provide a good compromise between the cross-validation RMSE, the weighted RMSE (lowest value) and the number of rejected points.

### 6.2.3. The selected Transfer Function

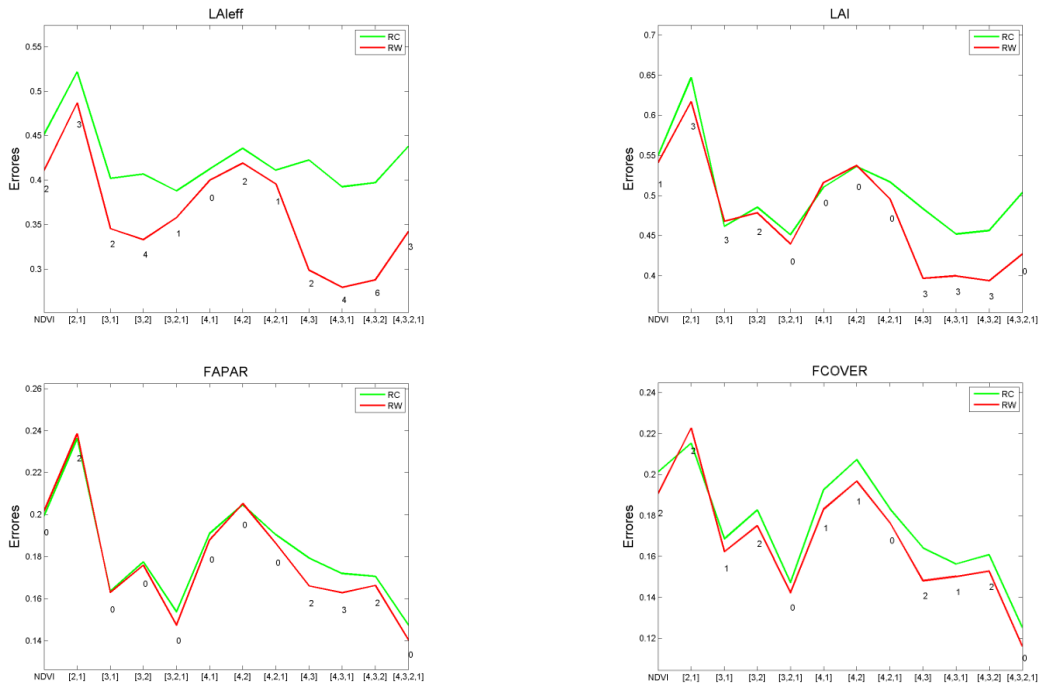
The applied transfer function for each variable is detailed in Table 7, along with its weighted and cross validated errors.

Very good TF are obtained, with low RMSE errors, lower than 0.5 for LAI except "third campaign", and RMSE errors between 0.05 and 0.15 for FAPAR/FCOVER. Higher errors are observed for LAI as compared to the LAI<sub>eff</sub> due to the larger uncertainties associated to the clumping estimation.

**Table 7: Transfer function applied to the whole site for LA<sub>leff</sub>, LAI and FAPAR. RW for weighted RMSE, and RC for cross-validation RMSE.**

Variable	Band Combination	RW	RC
<b>First Campaign</b>			
<b>LA<sub>leff</sub></b>	$3.85 - 0.0001 \cdot (\text{SWIR}) + 0.000157 \cdot (\text{NIR}) + 0.00064 \cdot (\text{R}) - 0.00104 \cdot (\text{G})$	0.34	0.44
<b>LAI</b>	$4.27 - 0.000117 \cdot (\text{SWIR}) + 0.00018 \cdot (\text{NIR}) - 0.000698 \cdot (\text{R}) - 0.0011 \cdot (\text{G})$	0.443	0.5
<b>FAPAR</b>	$1.799 - 0.000048 \cdot (\text{SWIR}) + 0.000079 \cdot (\text{NIR}) + 0.0003 \cdot (\text{R}) - 0.00049 \cdot (\text{G})$	0.14	0.149
<b>FCOVER</b>	$1.772 - 0.000061 \cdot (\text{SWIR}) + 0.000083 \cdot (\text{NIR}) + 0.00038 \cdot (\text{R}) - 0.00056 \cdot (\text{G})$	0.117	0.128
<b>Second Campaign</b>			
<b>LA<sub>leff</sub></b>	$2.601 - 0.023 \cdot (\text{SWIR}) - 0.033 \cdot (\text{NIR}) + 0.022 \cdot (\text{R}) + 0.035 \cdot (\text{G})$	0.274	0.431
<b>LAI</b>	$2.842 - 0.0229 \cdot (\text{SWIR}) - 0.0342 \cdot (\text{NIR}) + 0.0168 \cdot (\text{R}) + 0.043 \cdot (\text{G})$	0.35	0.668
<b>FAPAR</b>	$-0.017 - 0.0023 \cdot (\text{SWIR}) + 0.0066 \cdot (\text{NIR}) - 0.0067 \cdot (\text{R}) + 0.0083 \cdot (\text{G})$	0.059	0.062
<b>FCOVER</b>	$-0.638 + 0.0018 \cdot (\text{SWIR}) + 0.0026 \cdot (\text{NIR}) - 0.0047 \cdot (\text{R}) + 0.0095 \cdot (\text{G})$	0.052	0.06
<b>Third Campaign</b>			
<b>LA<sub>leff</sub></b>	$4.845 - 0.081 \cdot (\text{SWIR}) - 0.209 \cdot (\text{NIR}) + 0.1936 \cdot (\text{R}) + 0.0435 \cdot (\text{G})$	0.371	0.66
<b>LAI</b>	$5.2067 - 0.1057 \cdot (\text{SWIR}) - 0.3106 \cdot (\text{NIR}) + 0.2827 \cdot (\text{R}) + 0.0702 \cdot (\text{G})$	0.369	1.227
<b>FAPAR</b>	$0.619 - 0.0052 \cdot (\text{SWIR}) + 0.0116 \cdot (\text{NIR}) - 0.013 \cdot (\text{R}) + 0.0049 \cdot (\text{G})$	0.031	0.036
<b>FCOVER</b>	$0.065 - 0.00046 \cdot (\text{SWIR}) + 0.0115 \cdot (\text{NIR}) - 0.016 \cdot (\text{R}) + 0.0067 \cdot (\text{G})$	0.05	0.055
<b>Fourth Campaign</b>			
<b>LA<sub>leff</sub></b>	$8.211 - 0.0003 \cdot (\text{SWIR}) + 0.0003 \cdot (\text{NIR}) + 0.0016 \cdot (\text{R}) - 0.00237 \cdot (\text{G})$	0.28	0.39
<b>LAI</b>	$11.883 - 0.0003 \cdot (\text{SWIR}) + 0.00035 \cdot (\text{NIR}) + 0.002 \cdot (\text{R}) - 0.0032 \cdot (\text{G})$	0.55	0.65
<b>FAPAR</b>	$1.547 - 0.00005 \cdot (\text{SWIR}) + 0.00003 \cdot (\text{NIR}) - 0.000025 \cdot (\text{R}) - 0.00326 \cdot (\text{G})$	0.065	0.17
<b>FCOVER</b>	$0.3124 - 0.000005 \cdot (\text{SWIR}) + 0.000037 \cdot (\text{NIR}) - 0.0001 \cdot (\text{R}) - 0.00003 \cdot (\text{G})$	0.083	0.095
<b>Fifth Campaign</b>			
<b>LA<sub>leff</sub></b>	$11.08 + 0.000042 \cdot (\text{SWIR}) + 0.00016 \cdot (\text{NIR}) + 0.00078 \cdot (\text{R}) - 0.0021 \cdot (\text{G})$	0.4	0.6
<b>LAI</b>	$12.41 - 0.000087 \cdot (\text{SWIR}) + 0.00024 \cdot (\text{NIR}) + 0.0013 \cdot (\text{R}) - 0.0027 \cdot (\text{G})$	0.6	0.75
<b>FAPAR</b>	$2.52 - 0.0000044 \cdot (\text{SWIR}) + 0.000058 \cdot (\text{NIR}) + 0.00018 \cdot (\text{R}) - 0.00049 \cdot (\text{G})$	0.105	0.13
<b>FCOVER</b>	$1.99 + 0.000026 \cdot (\text{SWIR}) + 0.000033 \cdot (\text{NIR}) + 0.000044 \cdot (\text{R}) - 0.00031 \cdot (\text{G})$	0.04	0.095

### First Campaign (19<sup>th</sup>– 26<sup>th</sup> of June, 2013)



### Second Campaign (9<sup>th</sup> - 11<sup>th</sup> of July, 2013)

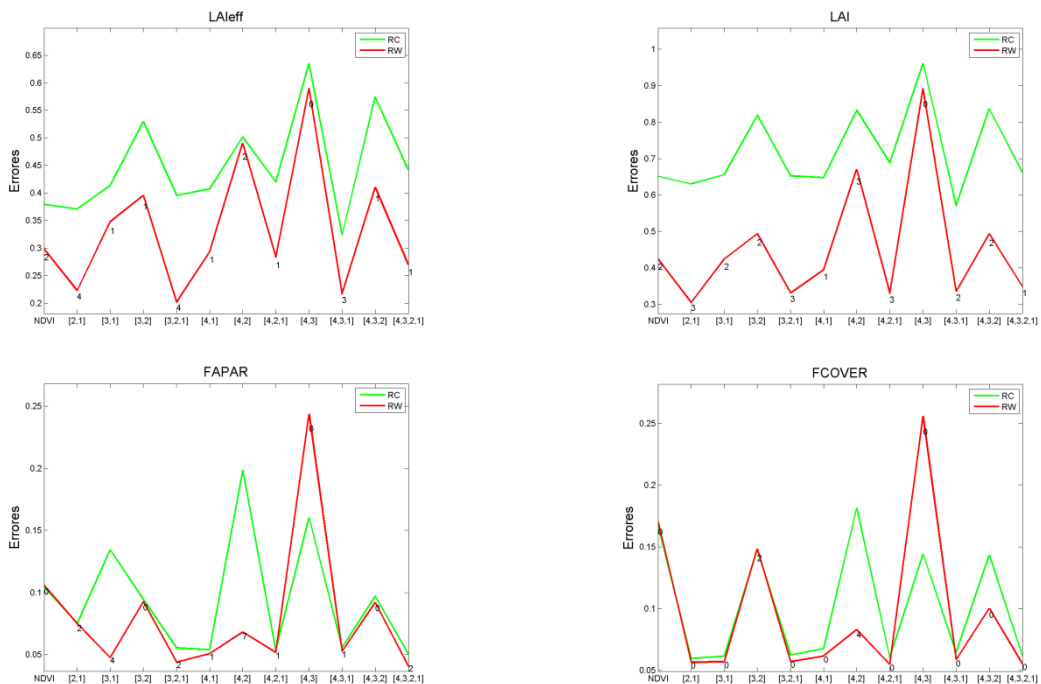
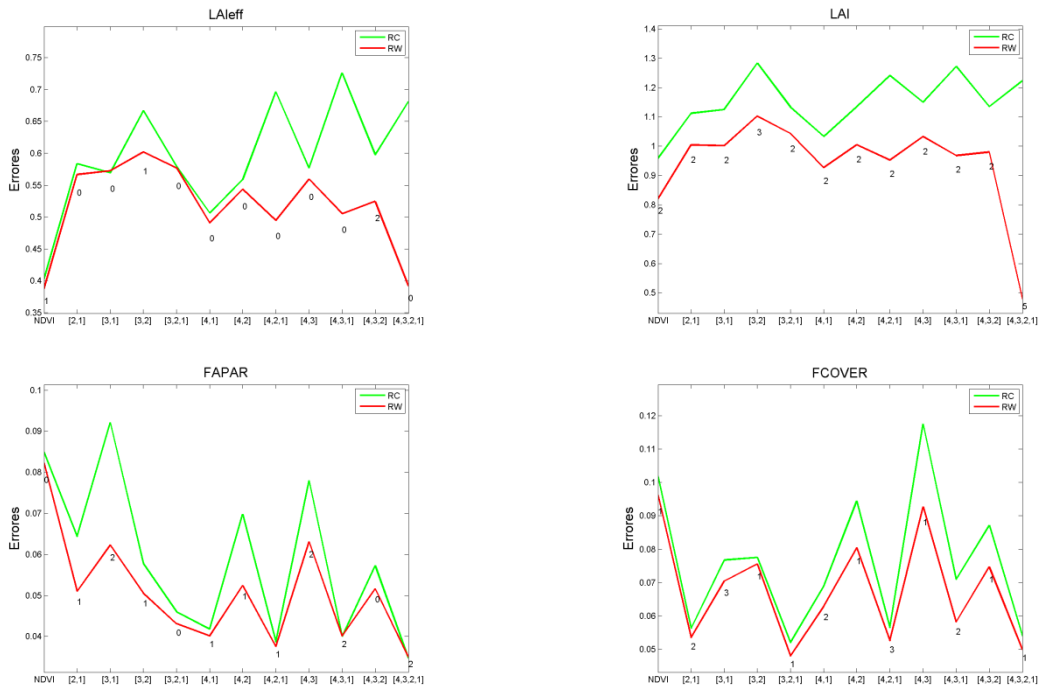


**Figure 9: Test of multiple regression(Transfer Function) applied on different band combinations. Band combinations are given in abscissa (1=G, 2=RED, 3=NIR and 4=SWIR). The weighted root mean square error (RMSE) is presented in red along with the cross-validation RMSE in green. The numbers indicate the number of data used for the robust regression with a weight lower than 0.7 that could be considered as outliers. Top: First campaign (19<sup>th</sup>– 26<sup>th</sup> of June, 2013). Bottom: Second campaign (9<sup>th</sup>– 11<sup>th</sup> of July, 2013)**

### Third Campaign (24<sup>th</sup> - 29<sup>th</sup> of July, 2013)



### Fourth Campaign (16<sup>th</sup> - 20<sup>th</sup> of August, 2013)

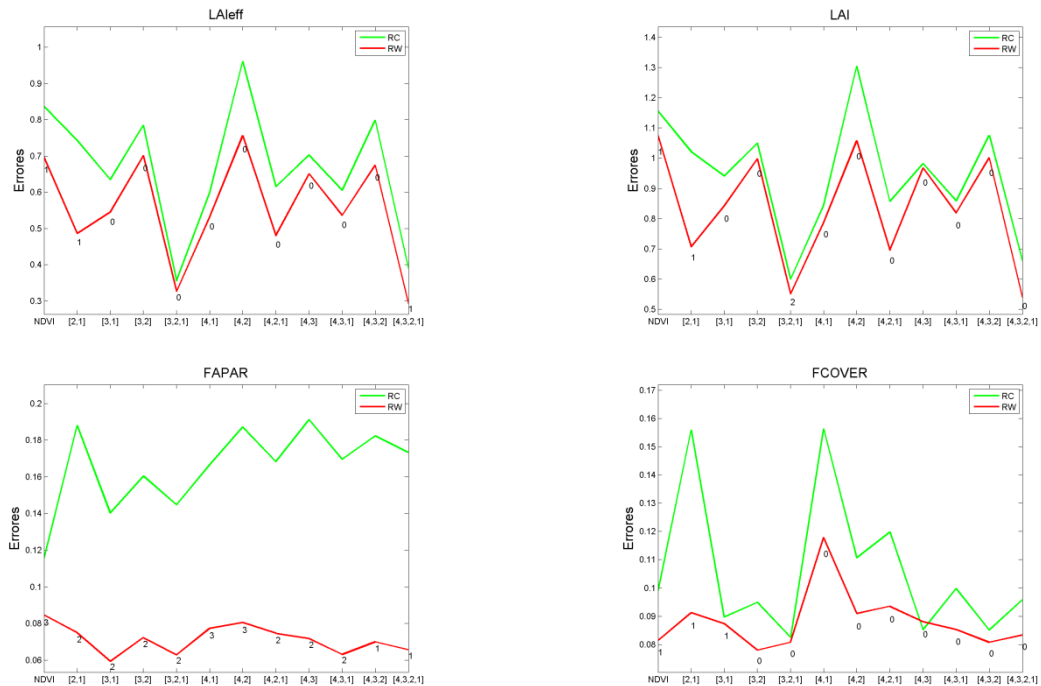


**Figure 10: Test of multiple regression (Transfer Function) applied on different band combinations. Band combinations are given in abscissa (1=G, 2=RED, 3=NIR and 4=SWIR). The weighted root mean square error (RMSE) is presented in red along with the cross-validation RMSE in green. The numbers indicate the number of data used for the robust regression with a weight lower than 0.7 that could be considered as outliers. Top: Third campaign (24<sup>th</sup>– 29<sup>th</sup> of July, 2013). Bottom: Fourth campaign (16<sup>th</sup>– 20<sup>th</sup> of August, 2013)**

### Fifth Campaign (2<sup>th</sup>- 6<sup>th</sup> of September, 2013)

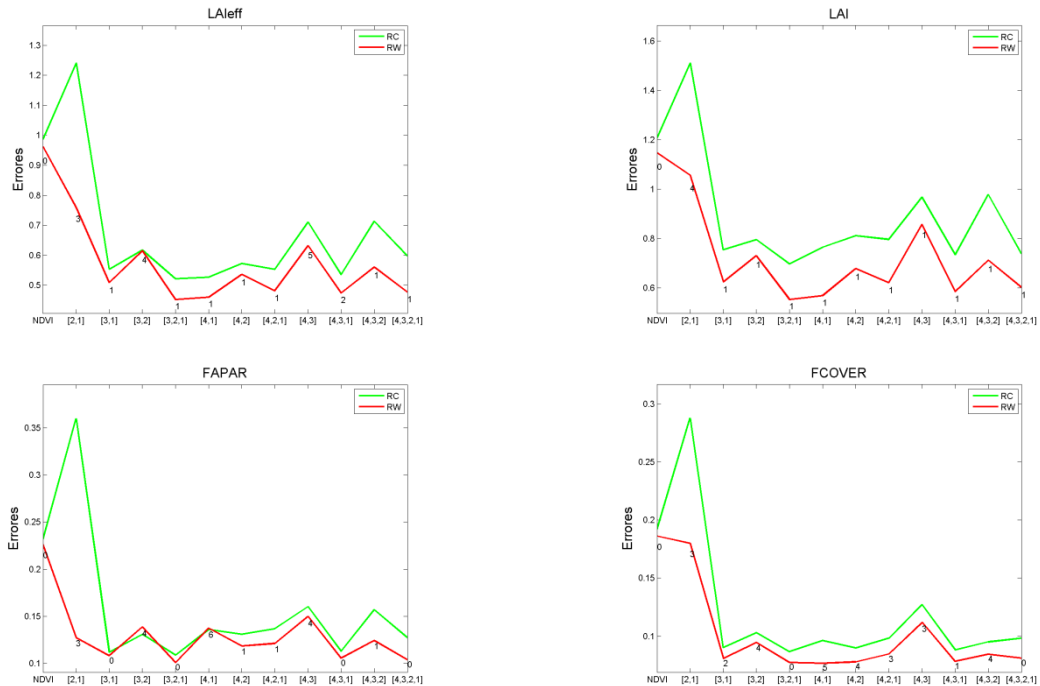


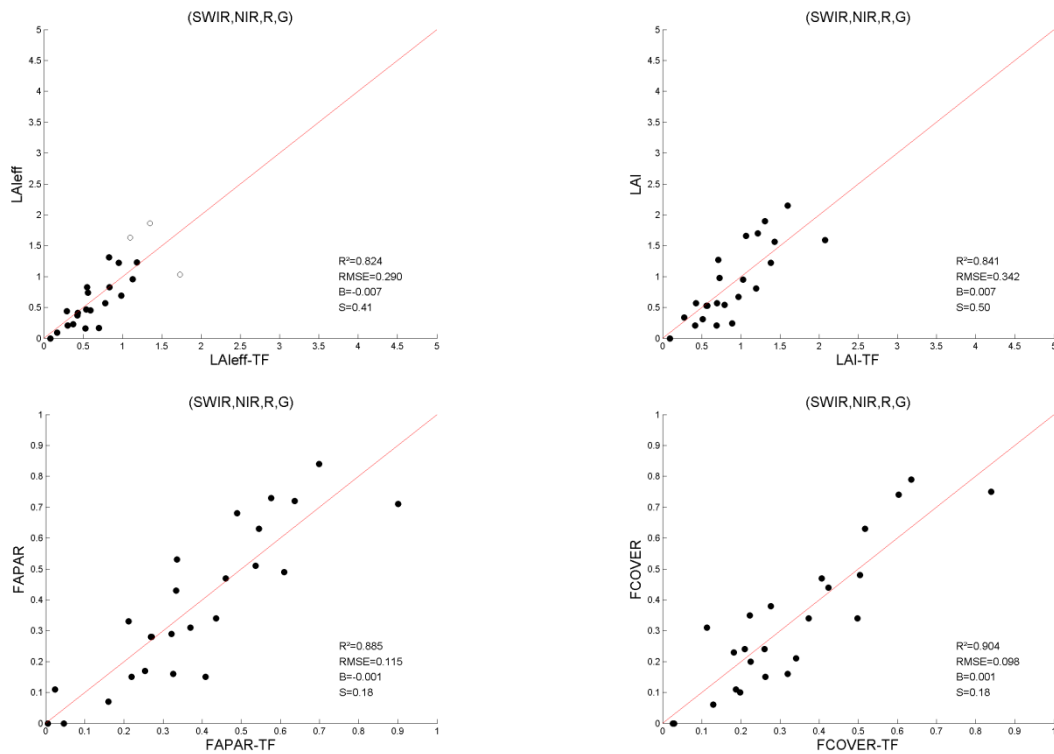
**Figure 11: Test of multiple regression(Transfer Function) applied on different band combinations. Band combinations are given in abscissa (1=G, 2=RED, 3=NIR and 4=SWIR). The weighted root mean square error (RMSE) is presented in red along with the cross-validation RMSE in green. The numbers indicate the number of data used for the robust regression with a weight lower than 0.7 that could be considered as outliers. Fifth campaign (2<sup>th</sup> – 6<sup>th</sup> of September, 2013).**

Figures 12, 13 and 14 show scatter-plots between ground observations and their corresponding transfer function (TF) estimates for the selected bands combinations.

Very good scatter-plots were obtained. A good correlation was observed for the LAIeff, LAI, FAPAR and FCOVER with points distributed along the 1:1 line, and with no bias and low RMSE errors.



### First Campaign (19<sup>th</sup>– 26<sup>th</sup> of June, 2013)



### Second Campaign (9<sup>th</sup> - 11<sup>th</sup> of July, 2013)

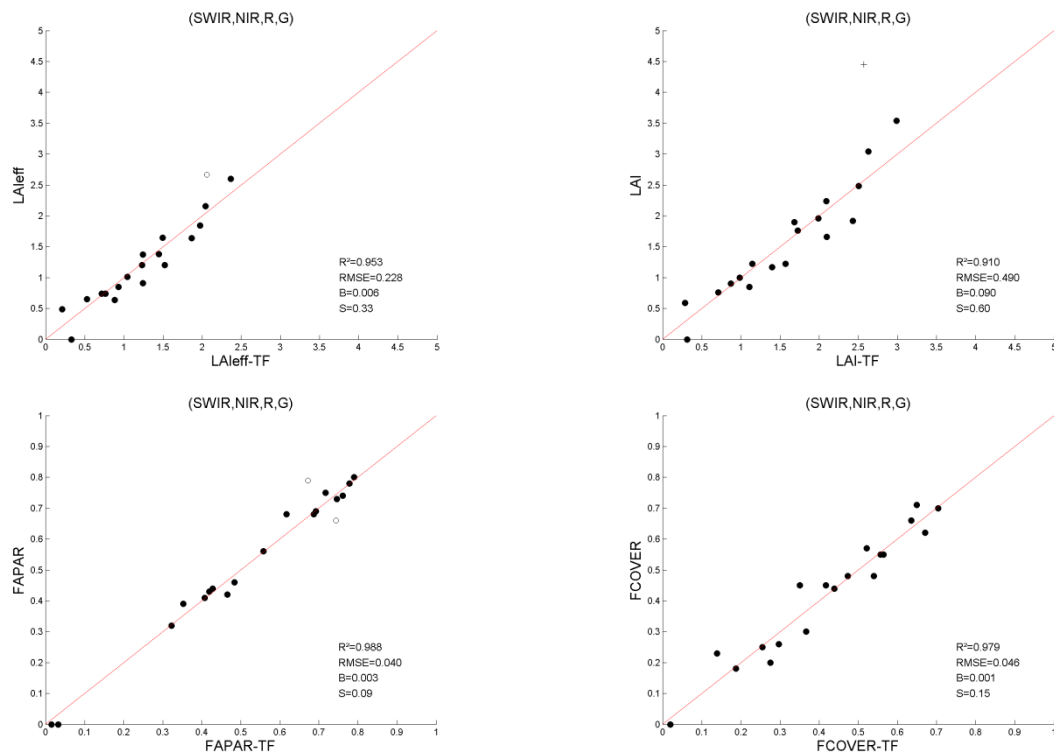
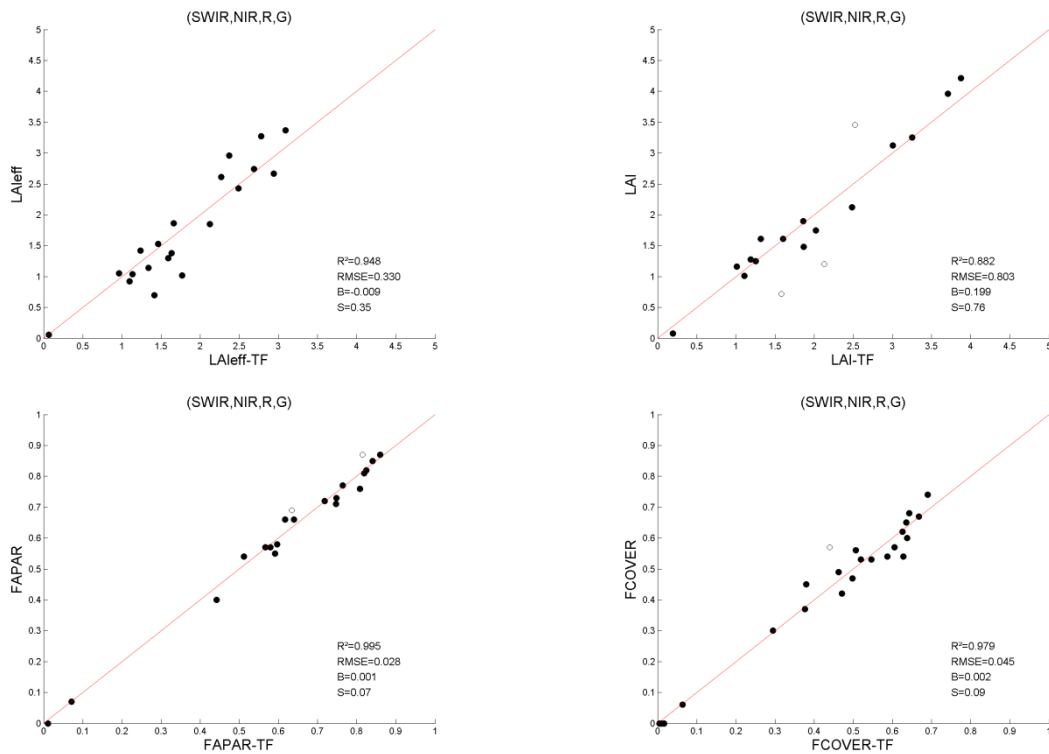


**Figure 12: LAleff, LAI, FAPAR and FCOVER: results for regression on reflectance using 4 bands combination. Full dots: Weight>0.7. Empty dots: 0<Weight<0.7. Crosses (if any): Weight=0. Top: First campaign (19<sup>th</sup>– 26<sup>th</sup> of June, 2013). Bottom: Second campaign (9<sup>th</sup>– 11<sup>th</sup> of July, 2013)**

### Third Campaign (24<sup>th</sup> - 29<sup>th</sup> of July, 2013)



### Fourth Campaign (16<sup>th</sup> - 20<sup>th</sup> of August, 2013)

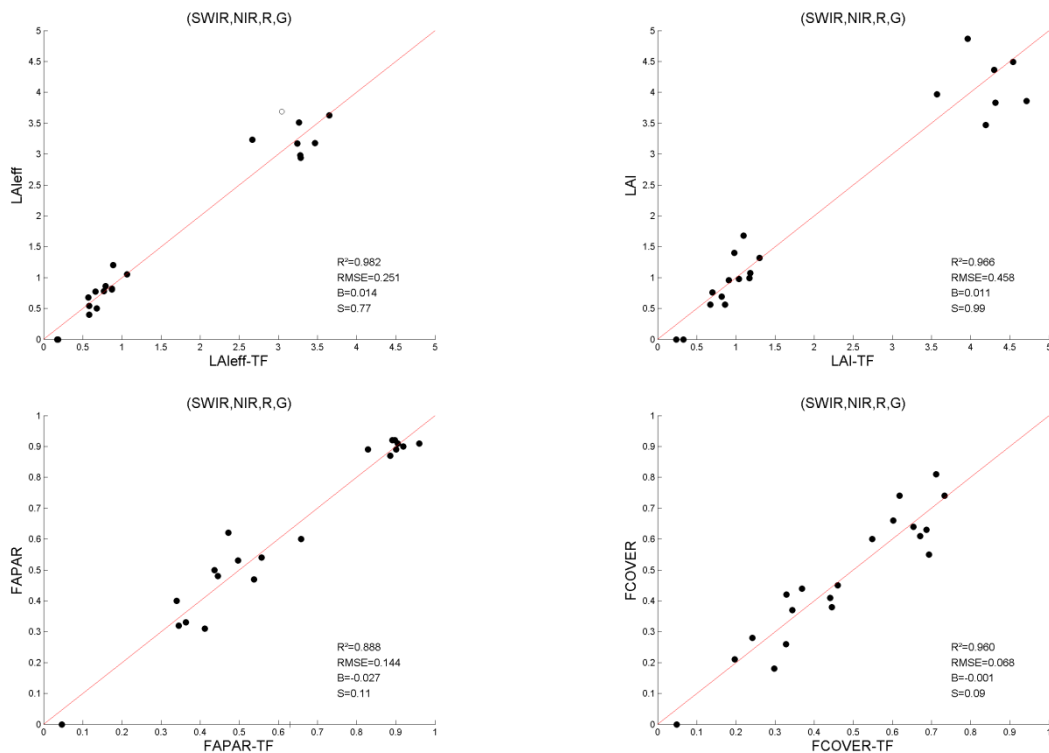
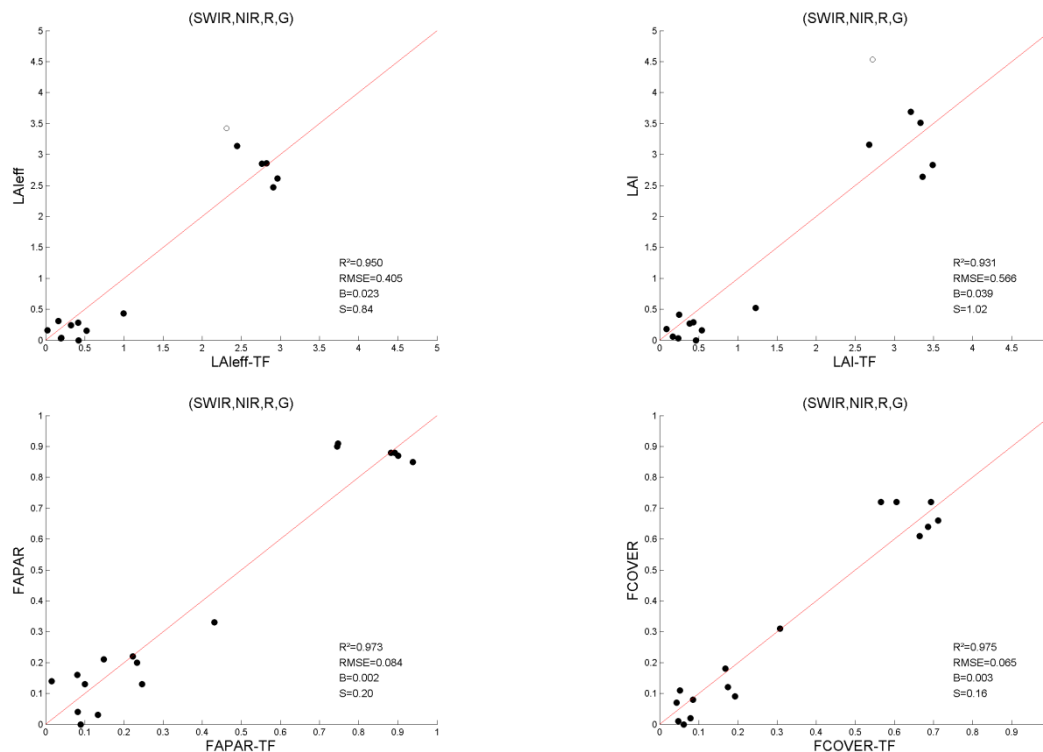


Figure 13: LAleff, LAI, FAPAR and FCOVER: results for regression on reflectance using 4 bands combination. Full dots: Weight>0.7. Empty dots: 0<Weight<0.7. Crosses (if any): Weight=0. Top: Third campaign (24<sup>th</sup>– 29<sup>th</sup> of July, 2013). Bottom: Fourth campaign (16<sup>th</sup>– 20<sup>th</sup> of August, 2013)

### Fifth Campaign (2<sup>th</sup>- 6<sup>th</sup> of September, 2013)



**Figure 14: LAleff, LAI, FAPAR and FCOVER: results for regression on reflectance using 4 bands combination. Full dots: Weight>0.7. Empty dots: 0<Weight<0.7. Crosses (if any): Weight=0. Fifth campaign (2<sup>th</sup> – 6<sup>th</sup> of September, 2013).**

## 6.3 THE HIGH RESOLUTION GROUND BASED MAPS

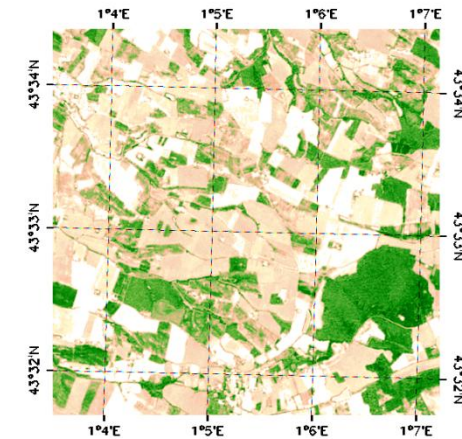
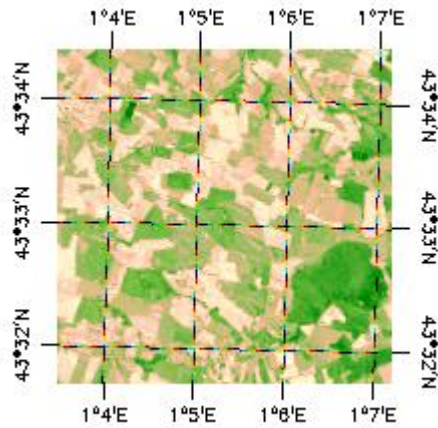
The high resolution ground based maps are obtained applying the selected transfer function of each variable (Table 7) to the SPOT5 and LANDSAT8 TOA reflectances. Figures 15 and 16 present the TF biophysical variables over the SW1 validation area for LAI and FAPAR, and figures 17 and 18 present the same LAI and FAPAR biophysical variables for the SW2 validation area. Similar results are obtained for LAleff (highly correlated to LAI) and FCOVER (highly correlated to FAPAR). The Quality Flags included in the final products are presented in figure 8. Note that the maps were calculated applying the selected band combination on a 5x5 km<sup>2</sup> area, but the means values for validation were computed over an 3x3 km<sup>2</sup> area.

The biophysical maps were found consistent among them, even for those plots where the transfer function behaves as extrapolator (QF=0), with the exception of the third campaign where the LAI products appears more noisy, and some inconsistencies with FAPAR/FCOVER were found where QF=0. Nevertheless, the mean values of LAI for the third campaign are consistent as compared with the temporal trend of the other parameters (Table 8). Moreover, we have derived a new transfer function map based on Landsat-8 (19 of July) for the third campaign, in order to check that the mean LAI values based on the

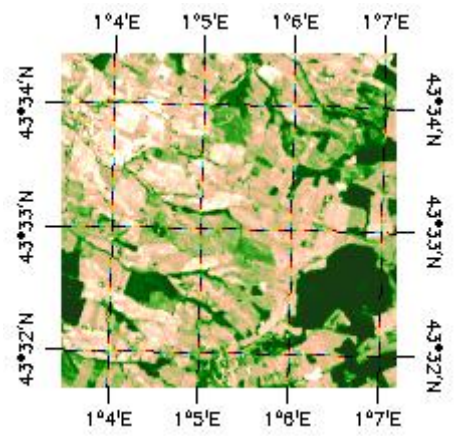
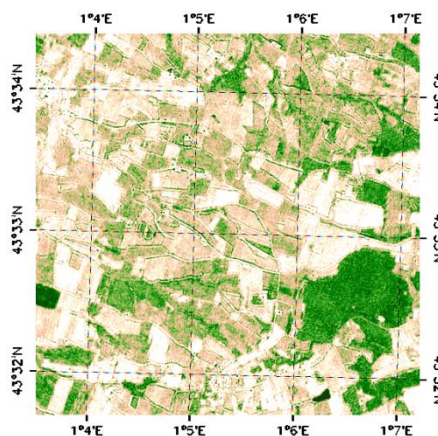
SPOT/VGT data are reliable ( see Annex I). As can be observed a very good agreement is found for all the biophysical parameters, with slight differences lower than 0.1 for LAI<sub>eff</sub> and 0.2 for LAI, and lower than 0.05 for FAPAR or FCOVER.

### LAI

**First Campaign (19<sup>th</sup>– 26<sup>th</sup> of June, 2013)**      **Second Campaign (9<sup>th</sup> - 11<sup>th</sup> of July, 2013)**



**Third Campaign (24<sup>th</sup> - 29<sup>th</sup> of July, 2013)**      **Fourth Campaign (16<sup>th</sup>-20<sup>th</sup> of August, 2013)**



**Fifth Campaign (2<sup>th</sup>- 6<sup>th</sup> of September, 2013)**

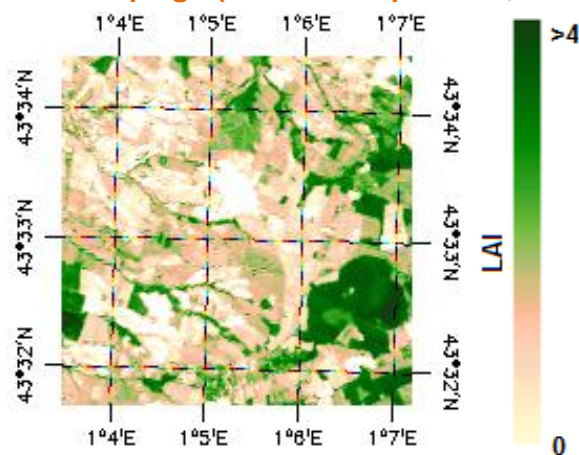
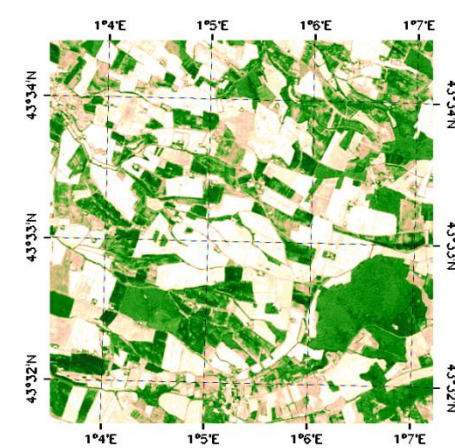
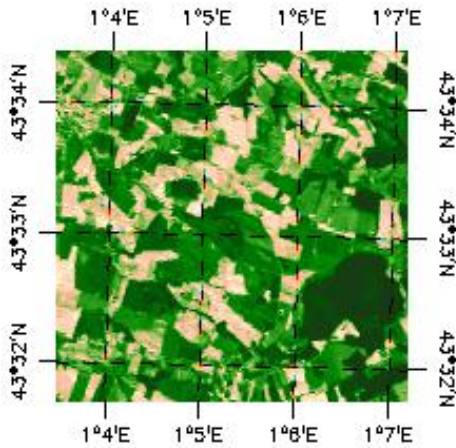


**Figure 15: Ground-based biophysical LAI maps applied on the 5x5 km<sup>2</sup> SW1 area for all the Campaigns. Second and Third campaign are based on SPOT-5, the others on LANDSAT-8.**

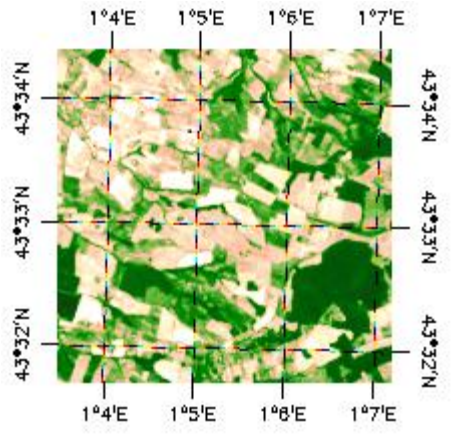
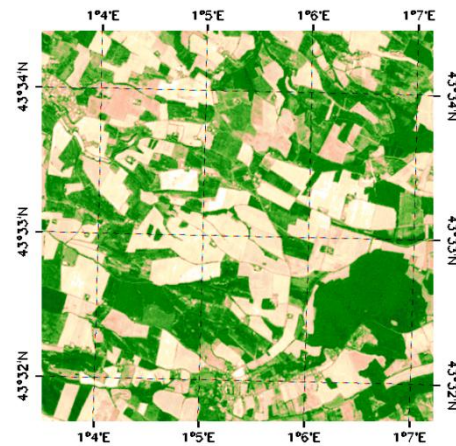


**FAPAR**

**First Campaign (19<sup>th</sup>– 26<sup>th</sup> of June, 2013)      Second Campaign (9<sup>th</sup> - 11<sup>th</sup> of July, 2013)**



**Third Campaign (24<sup>th</sup> - 29<sup>th</sup> of July, 2013)      Fourth Campaign (16<sup>th</sup>-20<sup>th</sup> of August, 2013)**



**Fifth Campaign (2<sup>th</sup>- 6<sup>th</sup> of September, 2013)**

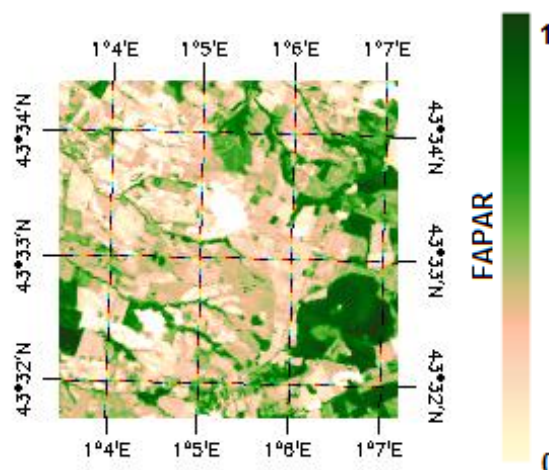
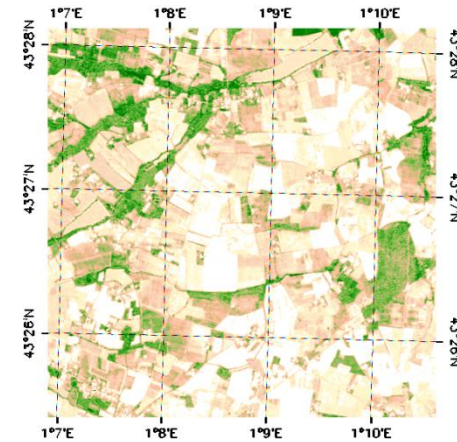
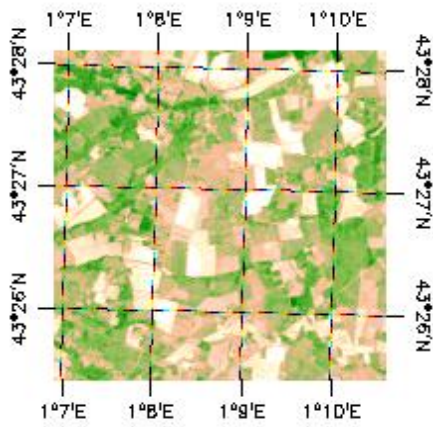


**Figure 16: Ground-based biophysical FAPAR maps applied on the 5x5 km<sup>2</sup> SW1 area for all the Campaigns. Second and Third campaign are based on SPOT-5, the others on LANDSAT-8.**

LAI

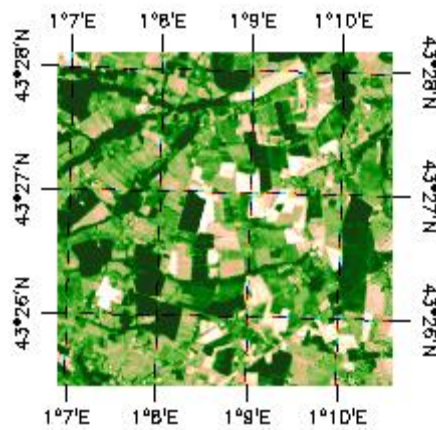
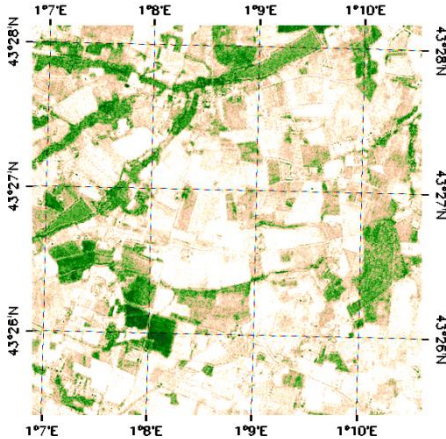
First Campaign (19<sup>th</sup>– 26<sup>th</sup> of June, 2013)

Second Campaign (9<sup>th</sup> - 11<sup>th</sup> of July, 2013)



Third Campaign (24<sup>th</sup> - 29<sup>th</sup> of July, 2013)

Fourth Campaign (16<sup>th</sup>-20<sup>th</sup> of August, 2013)



Fifth Campaign (2<sup>th</sup>- 6<sup>th</sup> of September, 2013)

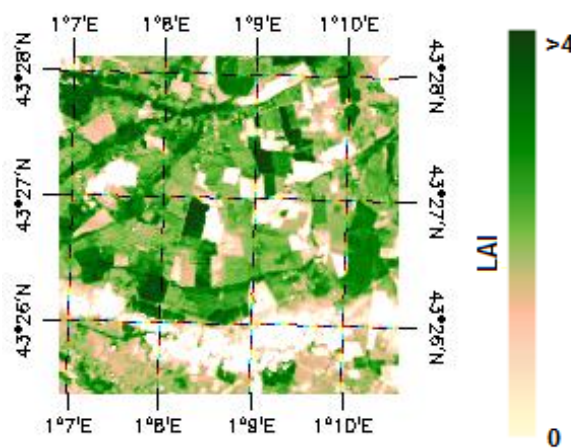
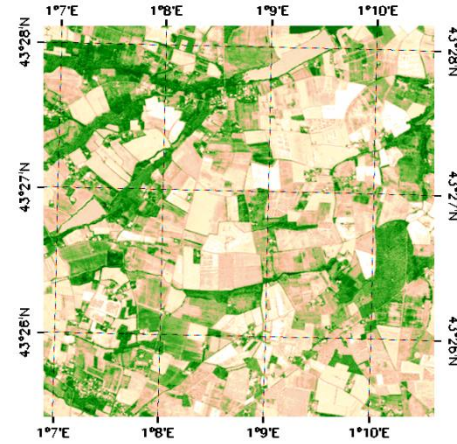
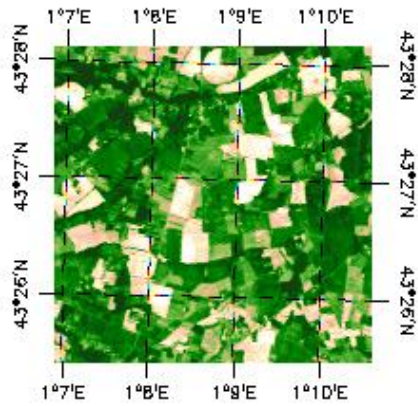


Figure 17: Ground-based biophysical LAI maps applied on the 5x5 km<sup>2</sup> SW2 area for all the Campaigns. Second and Third campaign are based on SPOT-5, the others on LANDSAT-8.

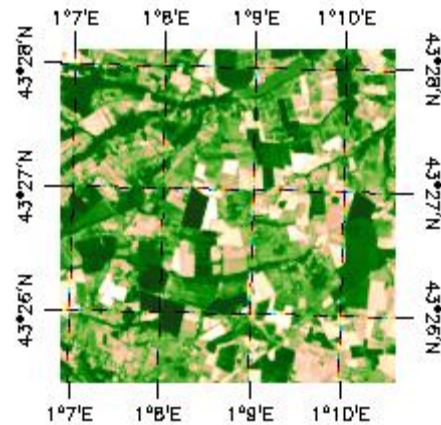
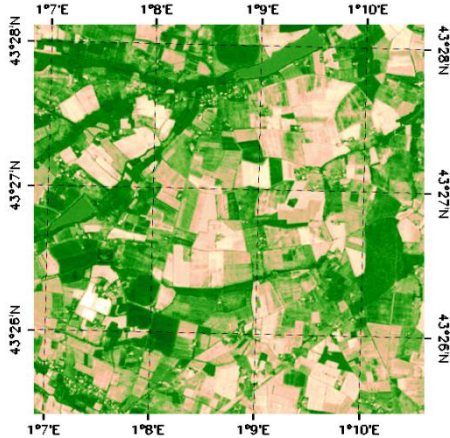


**FAPAR**

**First Campaign (19<sup>th</sup>– 26<sup>th</sup> of June, 2013)    Second Campaign (9<sup>th</sup> - 11<sup>th</sup> of July, 2013)**



**Third Campaign (24<sup>th</sup> - 29<sup>th</sup> of July, 2013)    Fourth Campaign (16<sup>th</sup>-20<sup>th</sup> of August, 2013)**



**Fifth Campaign (2<sup>th</sup>- 6<sup>th</sup> of September, 2013)**

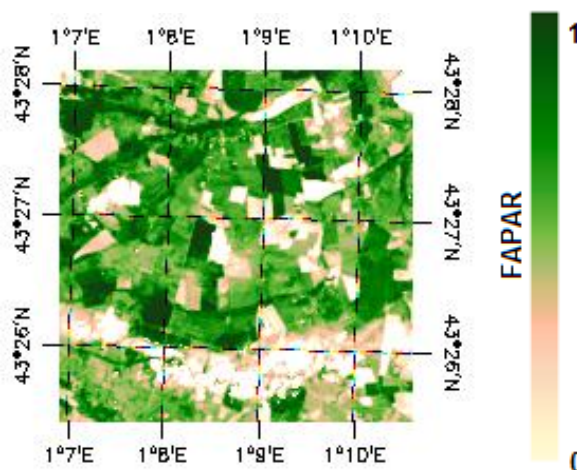


**Figure 18: HR biophysical FAPAR maps applied on the 5x5 km<sup>2</sup> SW2 area for all the Campaigns. Second and Third campaign are based on SPOT-5, the others on LANDSAT-8.**

Tables 8 and 9 summarize the mean values for the two "direct validation" 3x3 km<sup>2</sup> regions. Figures 19 and 20 show the temporal variations of these mean values. Note that the LAI for SW1 is not consistent with FAPAR and FCOVER for the fourth campaign. The behavior for this area is a smooth continuous decrease in the biophysical values between June and September 2013, and the large increase of LAI for campaign 4 seems not to be reliable, and should be discarded for validation. For the SW2, all variables are consistent, with a decrease between the first and second campaign (June and July), and an increase for the rest of campaigns (July, August, September) showing maximum values in August (four campaign). The exception was LA<sub>leff</sub> showing maximum values early September. This behavior can be explained due to the presence of summer crops (e.g. Maize) with maximum values around end of august (i.e., fourth campaign).

**Table 8: Mean values and standard deviation (STD) of the HR biophysical maps for the 3x3km<sup>2</sup> SouthWest site 1.**

SW1 (43.5511111° N, 1.088889° E)						
		First Campaign	Second Campaign	Third Campaign	Fourth Campaign	Fifth Campaign
		(19 <sup>th</sup> - 26 <sup>th</sup> of June, 2013)	(9 <sup>th</sup> - 11 <sup>th</sup> of July, 2013)	(24 <sup>th</sup> - 29 <sup>th</sup> of July, 2013)	(16 <sup>th</sup> -20 <sup>th</sup> of August,2013)	(2 <sup>th</sup> - 6 <sup>th</sup> of Sept, 2013)
LA <sub>leff</sub>	Mean	1.14	0.81	1	1.08	1.1
	STD	0.5	0.6	0.7	0.8	0.787
LAI	Mean	1.39	1.01	1.19	1.7 <sup>(*)</sup>	1.15
	STD	0.6	0.83	0.7	0.9	0.857
FAPAR	Mean	0.61	0.32	0.39	0.39	0.34
	STD	0.2	0.3	0.27	0.3	0.208
FCOVER	Mean	0.53	0.3	0.32	0.3	0.27
	STD	0.2	0.25	0.22	0.2	0.174

(\*) inconsistent with other parameters (discard)

**Table 9: Mean values and standard deviation (STD) of the HR biophysical maps for the 3x3km<sup>2</sup>SouthWest site 2.**

SW2 (43.44708° N, 1.14505° E)						
		First Campaign	Second Campaign	Third Campaign	Fourth Campaign	Fifth Campaign
		(19 <sup>th</sup> - 26 <sup>th</sup> of June, 2013)	(9 <sup>th</sup> - 11 <sup>th</sup> of July, 2013)	(24 <sup>th</sup> - 29 <sup>th</sup> of July, 2013)	(16 <sup>th</sup> -20 <sup>th</sup> of August,2013)	(2 <sup>th</sup> - 6 <sup>th</sup> of Sept, 2013)
LA <sub>leff</sub>	Mean	1.07	0.49	0.67	1.62	1.79
	STD	0.5	0.51	0.73	1	0.9
LAI	Mean	1.31	0.64	0.69	2.33	1.88
	STD	0.6	0.69	0.87	1.2	1
FAPAR	Mean	0.58	0.29	0.46	0.53	0.53
	STD	0.3	0.22	0.2	0.25	0.25
FCOVER	Mean	0.49	0.3	0.36	0.45	0.44
	STD	0.2	0.18	0.17	0.2	0.2



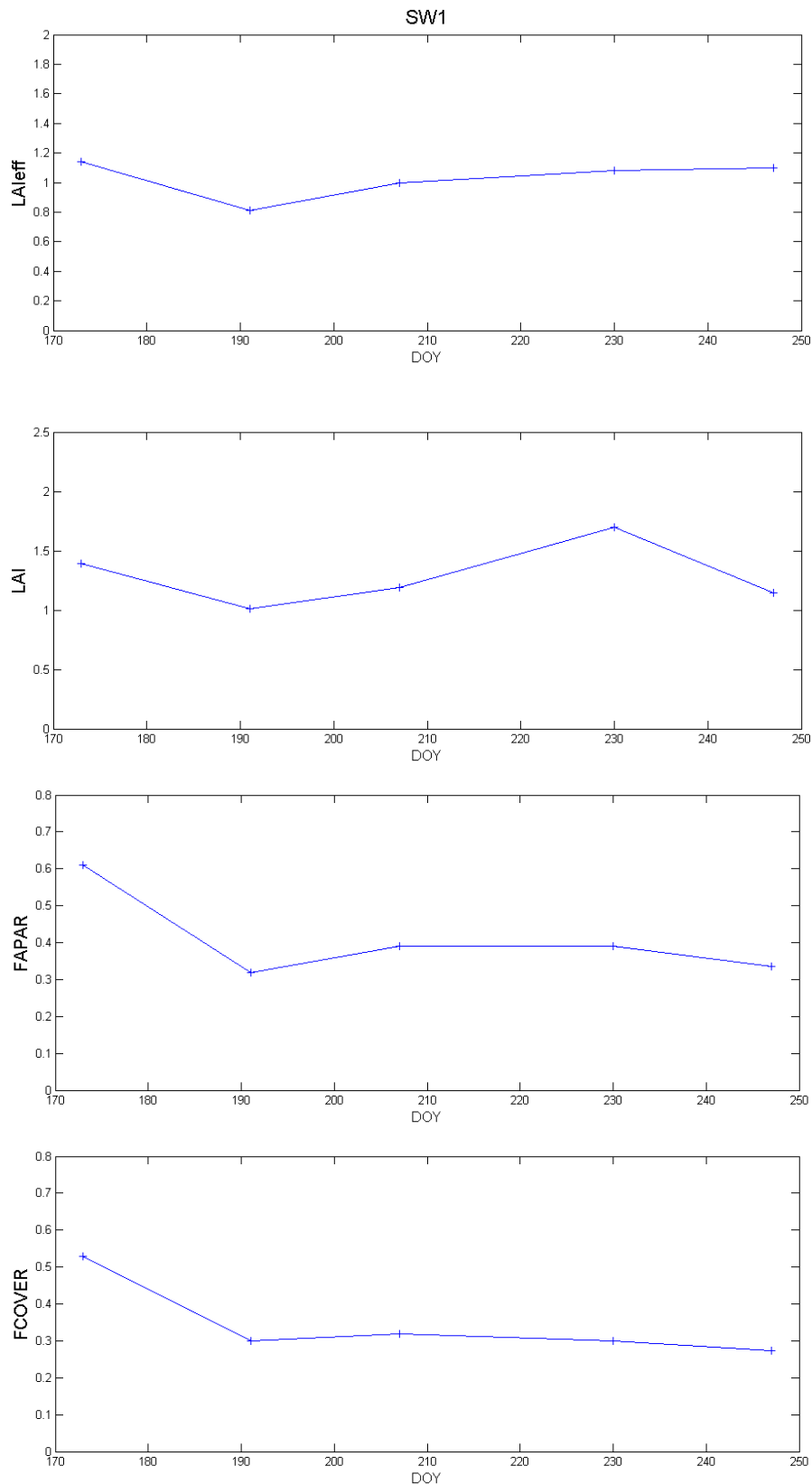


**Figure 19: Temporal variations of the mean values over SW1 3x3km<sup>2</sup> area for LAleff, LAI, FAPAR and FCOVER.**

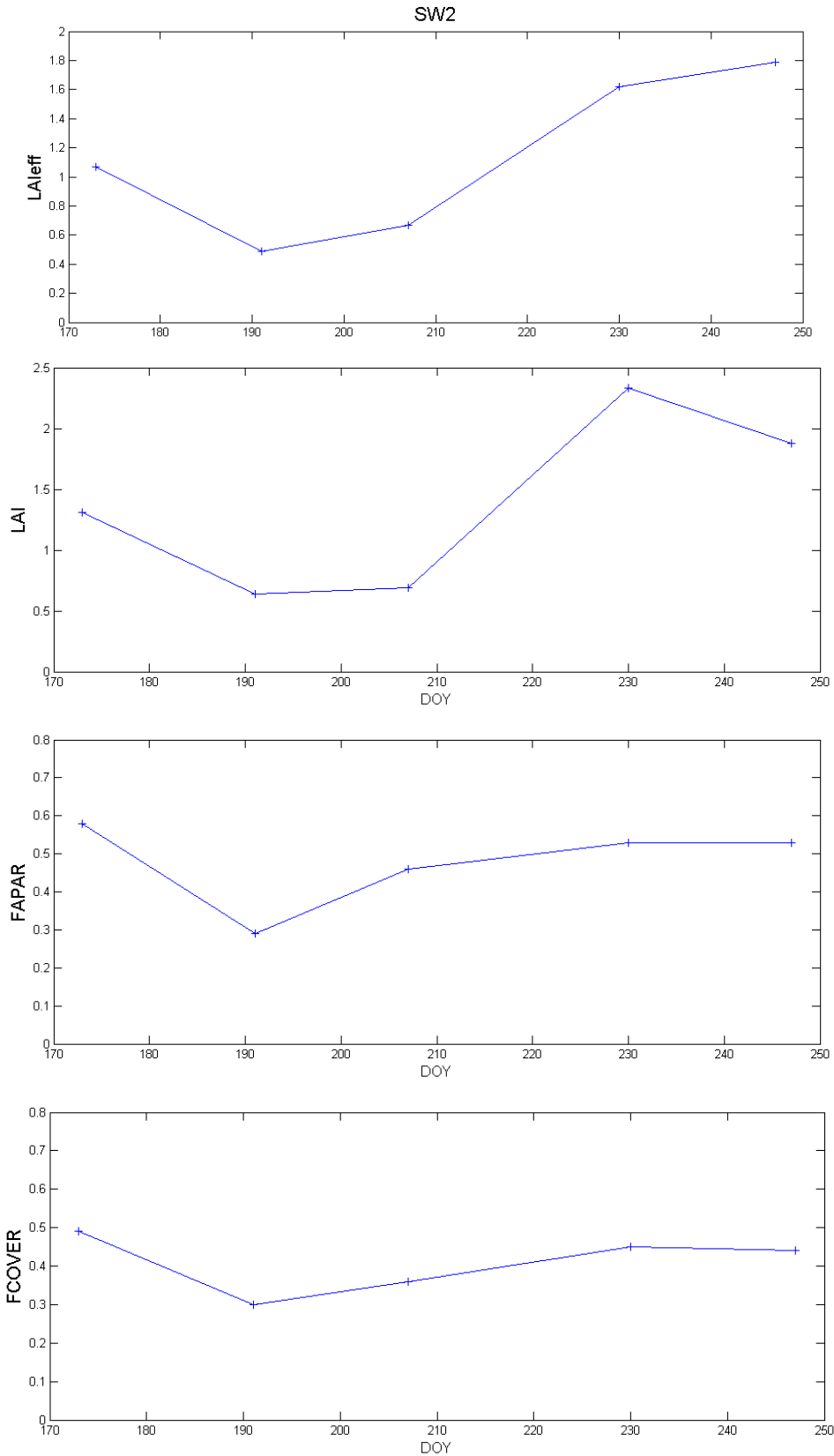


**Figure 20: Temporal variations of the mean values over SW2 3x3km<sup>2</sup> area for LAIeff, LAI, FAPAR and FCOVER.**

Table 10 describes the content of the biophysical maps in the “BIO\_YYYYMMDD\_SENSOR\_ZONE ETF\_Area” files.

where:

BIO stands for Biophysical (LAI, FAPAR, FCOVER)

YYYYMMDD = date

SENSOR = LANDSAT8 or SPOT5

ZONE = SW1 or SW2

ETF stands for Empirical Transfer Function

Area = window size (km x km)

**Table 10: Content of the dataset.**

Parameter	Dataset name	Range	Variable Type	Scale Factor	No Value
<b>LAIeffective</b>	LAIeff	[0, 7]	Integer	1000	-1
<b>LAI</b>	LAI	[0, 7]	Integer	1000	-1
<b>FAPAR</b>	FAPAR	[0, 1]	Integer	10000	-1
<b>FCOVER</b>	FCOVER	[0, 1]	Integer	10000	-1
<b>Quality Flag</b>	QFlag	0,1,2 (*)	Integer	N/A	-1

(\*)0 means extrapolated value (low confidence), 1 strict interpolator (best confidence), 2 large interpolator

## 7. CONCLUSIONS

Ground based high resolution maps of main biophysical variables of the vegetation canopy have been derived over the agriculture area of SouthWest (France) from multi-temporal ground data for five selected periods or "ground campaigns" centered around: 22<sup>th</sup> of June, 10<sup>th</sup> of July, 26<sup>th</sup> of July, 18<sup>th</sup> of August and 4<sup>th</sup> of September 2013. The ground-based maps were derived according with the CEOS LPV recommendations for validation of low resolution satellite sensors. The main conclusions are the following:

- **Ground data**

Ground data were acquired using digital hemispherical photographs, and processed with the CAN-EYE software to provide LAI, LAI<sub>eff</sub>, FAPAR and FCOVER values. Green values are considered. Three main crops were sampled: One spring crop (wheat) in a senescent state in "Campaign 1", and two summer crops (sunflower and maize) with maximum values during the summer.

- **Sampling and Quality Flag**

The sampling over the 20x20 km<sup>2</sup> study area is located northwest and southwest of the central coordinate, because of this two homogeneous areas of 3x3km<sup>2</sup> were chosen to provide the mean values for direct validation. These two areas are located to the east (SW1) and south (SW2) of the central coordinate over homogeneous croplands, avoiding the many urban areas existing in the region and the water bodies. The sampling over the study area was evaluated with the convex hull test. Due to the low number of crop types sampled (Maize, Wheat and Sunflower) and the heterogeneity of the study area, only a percentage between 25% and 51% (whole site, 20x20 km<sup>2</sup>) belongs to the transfer function considered as an interpolator. The information provided in the Quality Flag should be carefully considered. The representativeness of the sampling is slightly better over the two validated 3x3km<sup>2</sup> areas, ranging typically between 40 and 60%. However the 3x3 km<sup>2</sup> are cropland areas, and the several biophysical maps were found consistent and reliable also where the TF behaves as extrapolator (QF=0). The only exception was the LAI products in campaign 3 where some inconsistencies were detected (for QF=0), but without showing the mean value a consistent temporal behavior than other products, as well as consistent with LAI values up-scaled with Landsat-8 data for the same ground dataset (Annex II).

- **The Transfer Function**

Transfer functions have been derived by multiple robust regression between ESUs TOA reflectance using SPOT-5 and LANDSAT 8 imagery and the several biophysical variables. The spectral bands combination to minimize errors (weighted RMSE and cross-validation RSME) were band 1 (green), band 2 (red) band 3 (Near Infrared) and band 4 (Short Wave Infrared) combination, for all campaigns and parameters. The RMSE values for the several transfer function estimates are ranging between 0.29 and 0.38 for LAI<sub>eff</sub>, 0.34 and 0.8 for

LAI, 0.04 and 0.11 for FAPAR, and finally 0.03 and 0.1 for FCOVER. The results are good for the five field campaigns, with no bias and low RMSE.

- ***Ground based maps and Mean Values for validation***

The biophysical variable maps are provided over a 5x5 km<sup>2</sup> area in UTM, 31 North, projection coordinates (Datum: WGS-84) at 10m resolution (i.e., SPOT-5) for campaigns 2, and 3, and at 30m resolution (i.e., Landsat-8) for campaigns 1, 4 and 5, including the biophysical variables and the QF.

Mean values and standard deviation for LAI<sub>eff</sub>, LAI, FAPAR and FCOVER were computed over the two selected 3x3 km<sup>2</sup> areas (Table 8 and Table 9). All values were found consistent, except LAI values for SW1 area during the campaign 4 that shows an unreliable large increase. This value is the only not recommended for validation.

## 8. ACKNOWLEDGEMENTS

This work is supported by the FP7 IMAGINES project under Grant Agreement N°311766. SPOT 5-HR imagery are provided through the GMES Services Coordinated Interface (SCI) ESA service. This work is done in collaboration with the consortium implementing the Global Component of the Copernicus Land Service.

Thanks to Valérie Demarez (David Morin, Marjorie Battude, Olivia Mas-Erauso, and J.F Dejoux) team at CESBIO for providing the ground data.

## 9. REFERENCES

- Baret, F., and Fernandes, R. (2012). Validation Concept. VALSE2-PR-014-INRA, 42 pp.
- Camacho, F., Cernicharo, J., Lacaze, R., Baret, F., and Weiss, M. (2013). GEOV1: LAI, FAPAR Essential Climate Variables and FCOVER global time series capitalizing over existing products. Part 2: Validation and intercomparison with reference products. *Remote Sensing of Environment*, 137: 310-329.
- Claverie, M., Vermote, E.F., Weiss, M., Baret, F., Hagolle, O., Demarez, V. (2013). Validation of coarse spatial resolution LAI and FAPAR time series over cropland in southwest France. *Remote Sensing of Environment*, 139: 216-230.
- Demarez, V., Duthoit, S., Baret, F., Weiss, M. and Dedieu, G. (2008). Estimation of leaf area and clumping indexes of crops with hemispherical photographs. *Agricultural and Forest Meteorology*. 148, 644-655.
- Fernandes, R. S. Plummer, F. Baret, G. Schaepman-Strub, J. Nickeson, J. Nightingale (2012). Global LAI Product Validation Protocol, v1.4. Committee of Earth Observing Systems Working Group on Calibration and Validation Land Product Validation Sub-Group (in revision).
- Martínez, B., García-Haro, F. J., & Camacho, F. (2009). Derivation of high-resolution leaf area index maps in support of validation activities: Application to the cropland Barrax site. *Agricultural and Forest Meteorology*, 149, 130–145.
- Morissette, J. T., Baret, F., Privette, J. L., Myneni, R. B., Nickeson, J. E., Garrigues, S., et al. (2006). Validation of global moderate-resolution LAI products: A framework proposed within the CEOS land product validation subgroup. *IEEE Transactions on Geoscience and Remote Sensing*, 44, 1804–1817.
- Weiss, M., Baret, F., Smith, G.J., Jonckheere, I. and Coppin, P., (2004). Review of methods for in situ leaf area index (LAI) determination. Part II. Estimation of LAI, errors and sampling. *Agricultural and Forest Meteorology*. 121, 37–53.



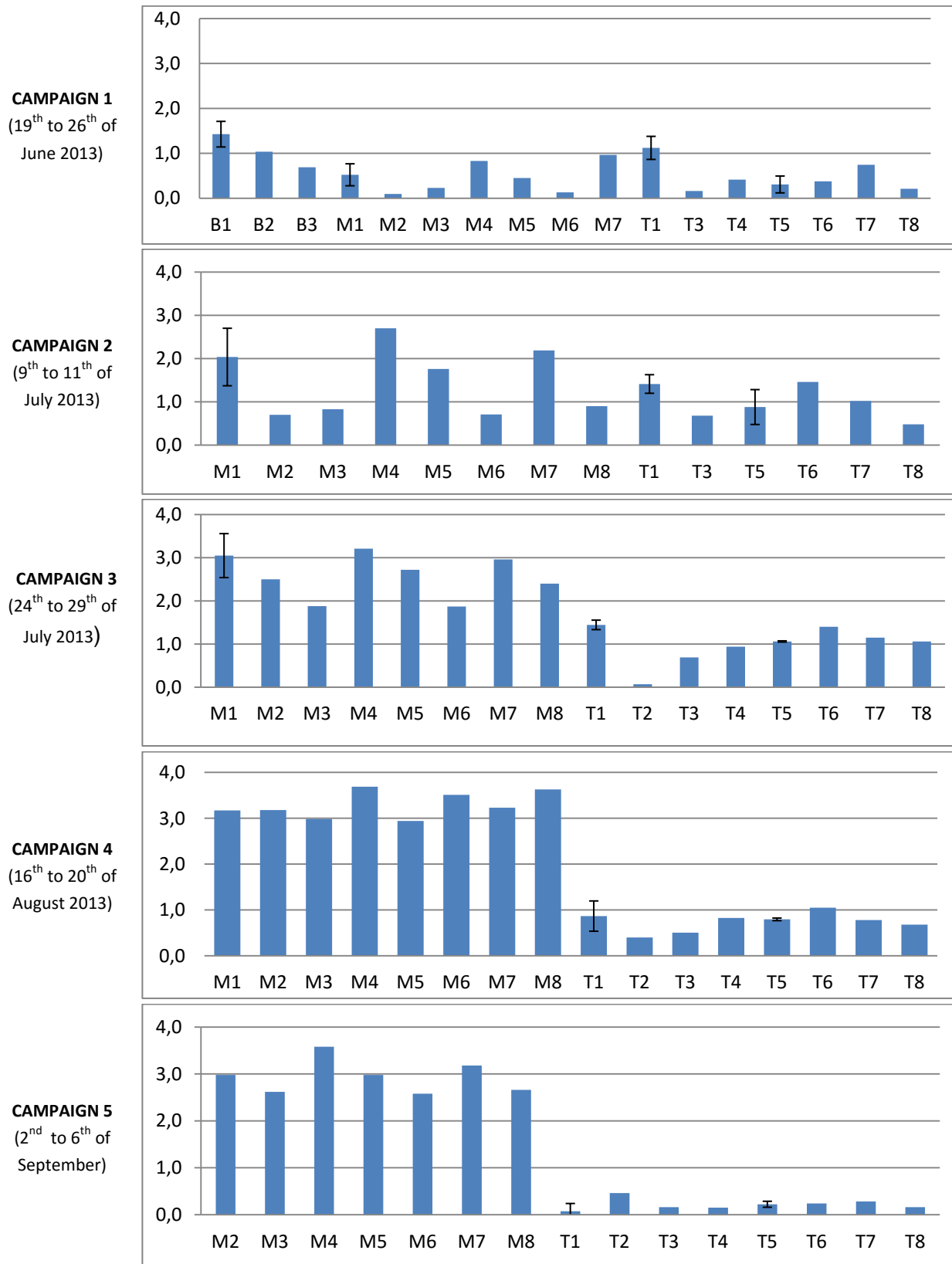




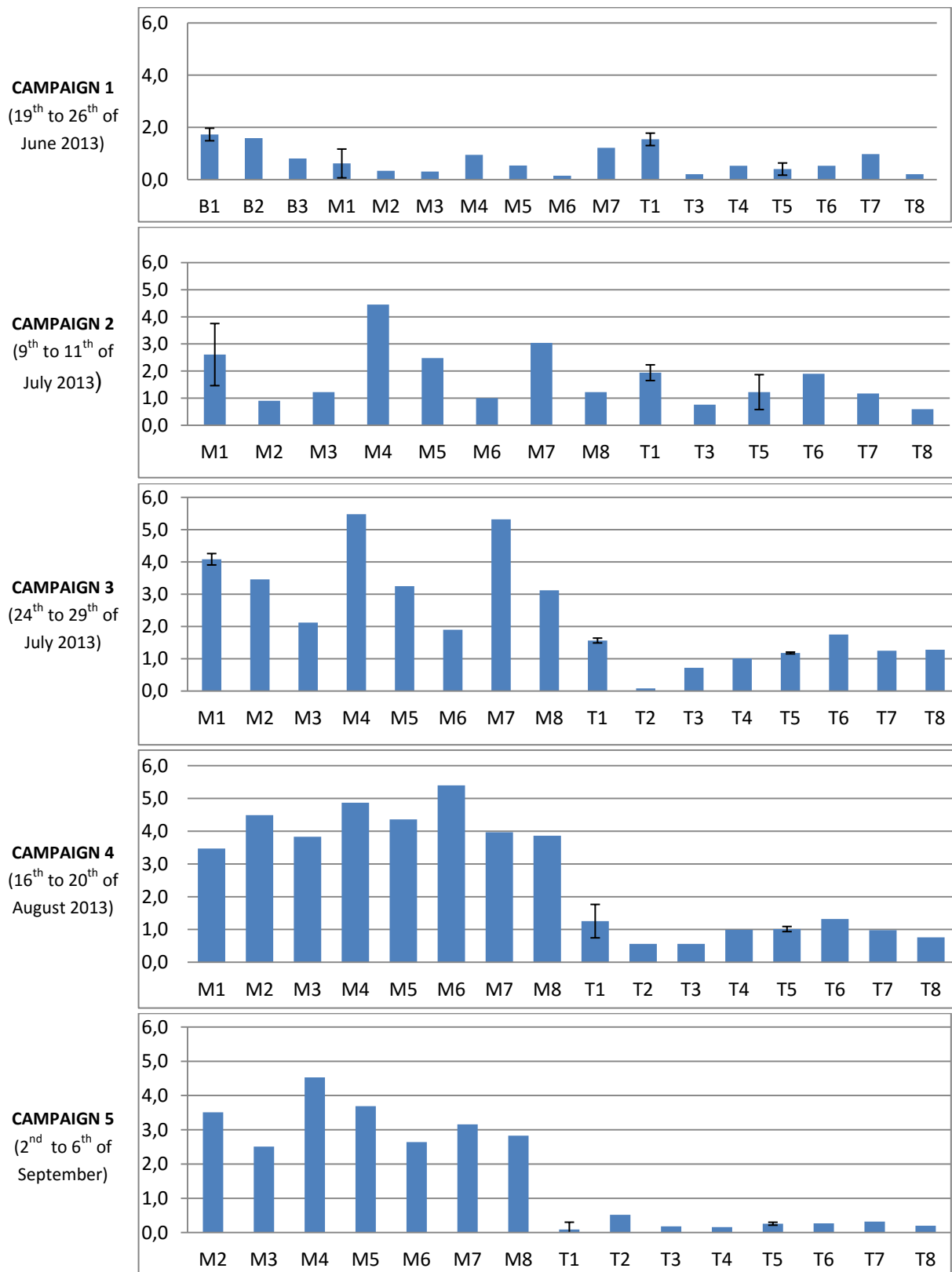


## **ANNEX I: STATISTICS OF GROUND DATA**

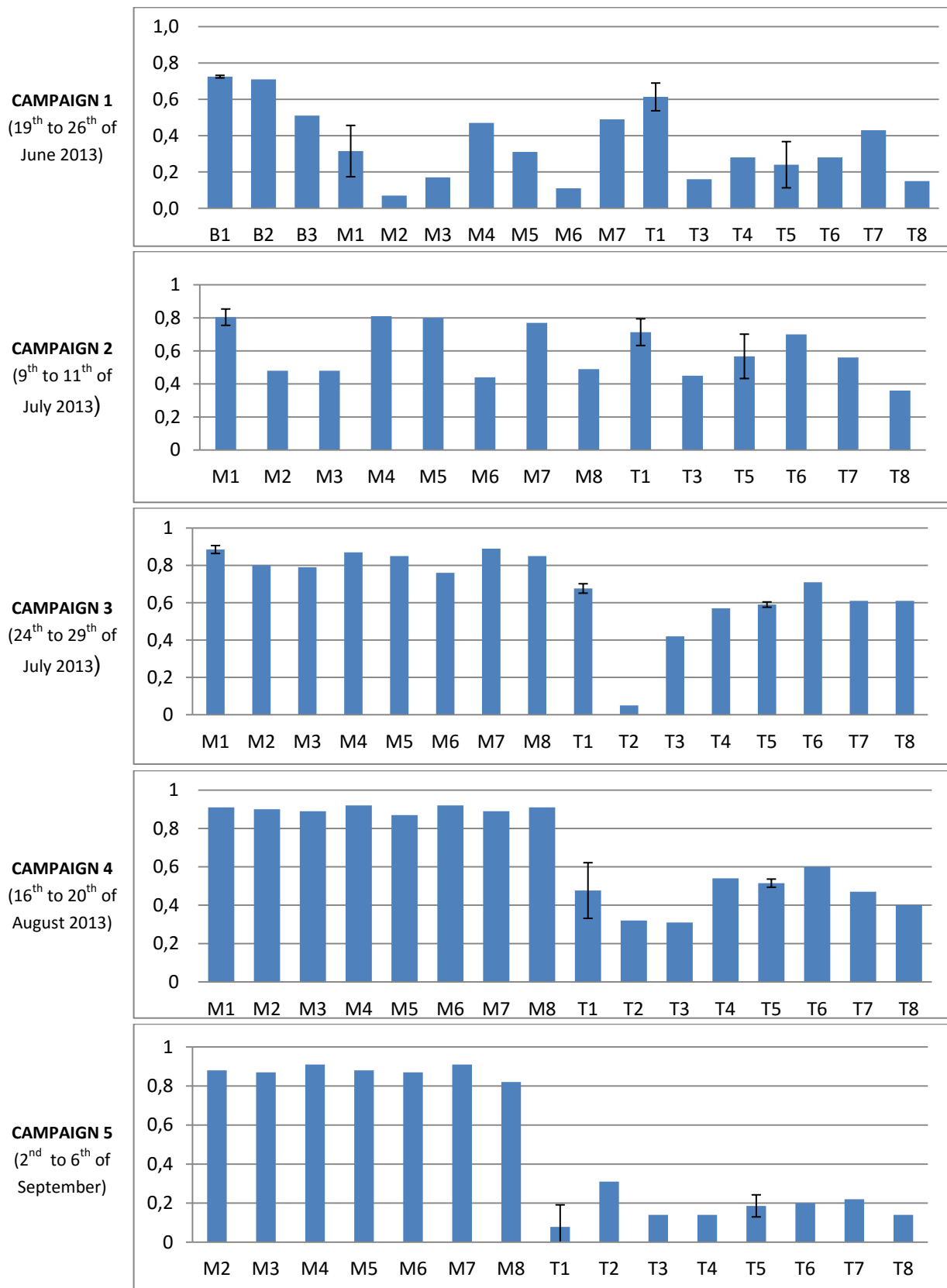
**LAleff**



### LAI

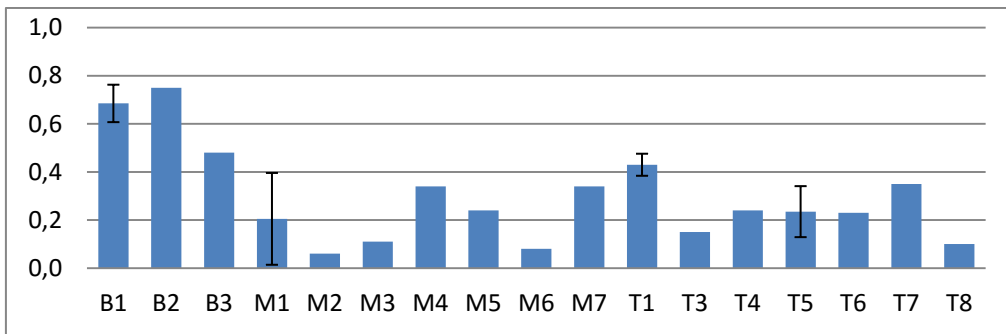


### FAPAR

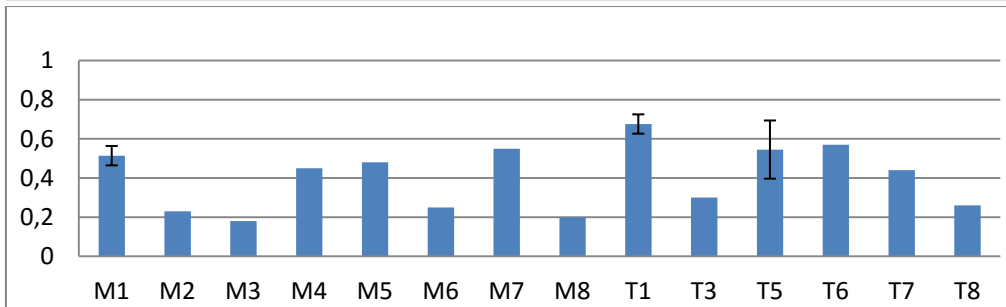


### FCOVER

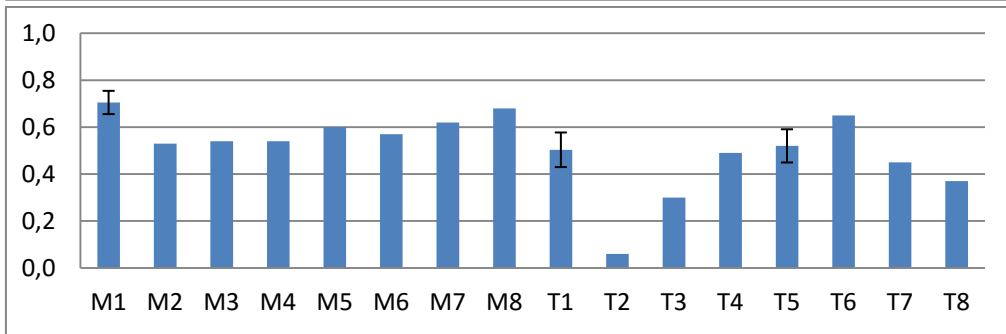
**CAMPAIGN 1**  
 (19<sup>th</sup> to 26<sup>th</sup>  
 of June 2013)



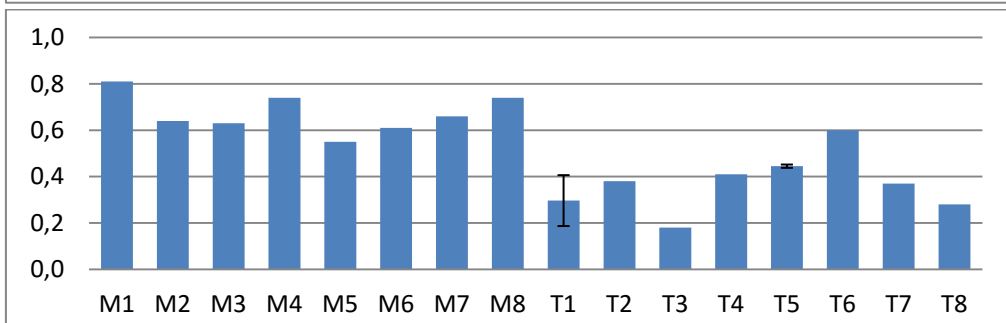
**CAMPAIGN 2**  
 (9<sup>th</sup> to 11<sup>th</sup> of  
 July 2013)



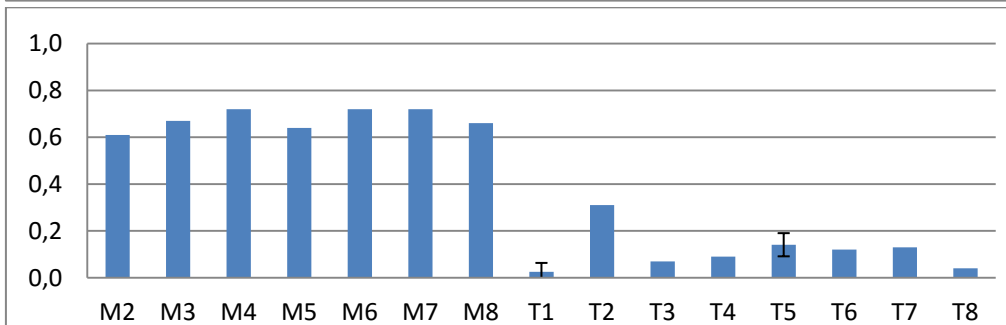
**CAMPAIGN 3**  
 (24<sup>th</sup> to 29<sup>th</sup>  
 of July 2013)



**CAMPAIGN 4**  
 (16<sup>th</sup> to 20<sup>th</sup>  
 of August  
 2013)

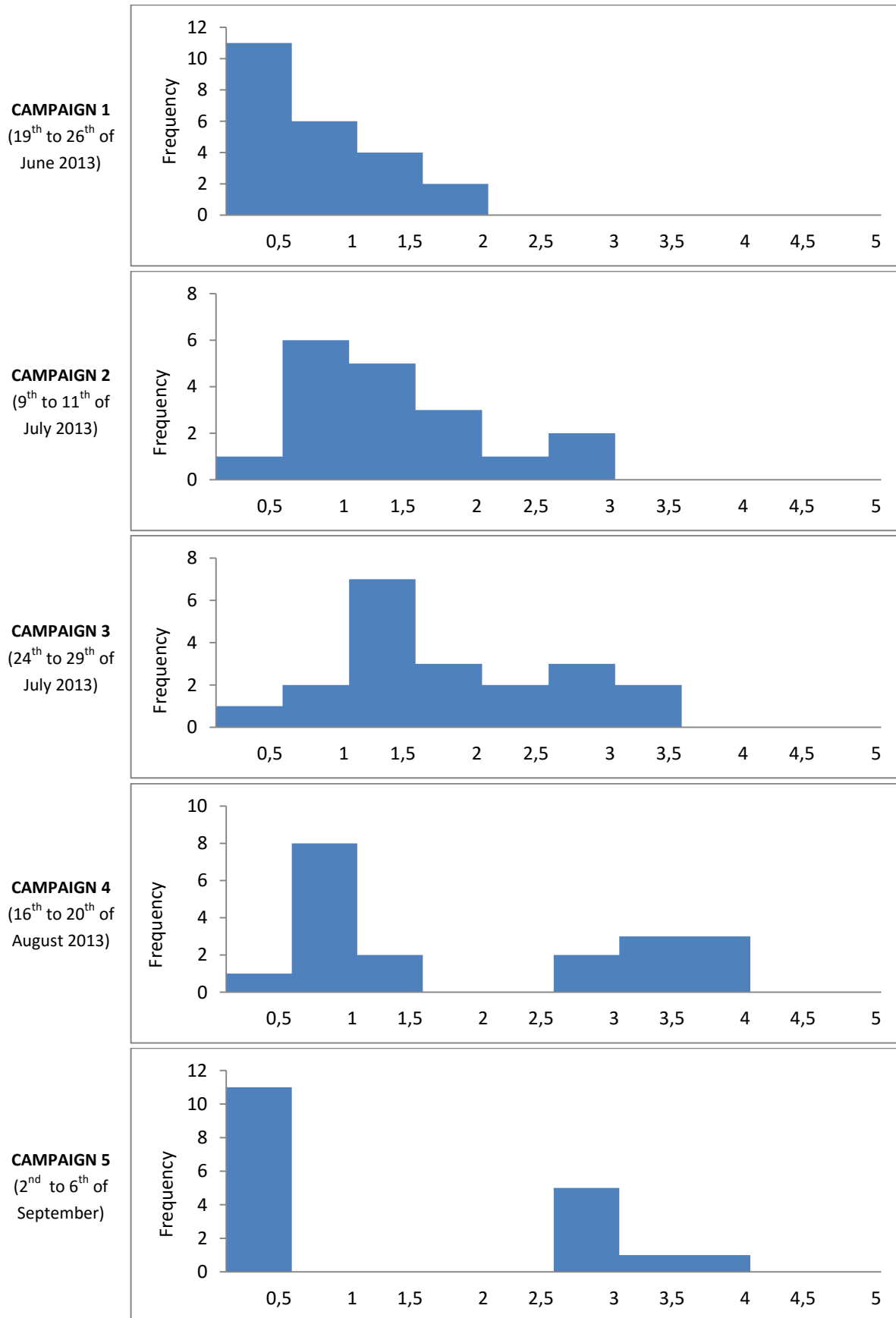


**CAMPAIGN 5**  
 (2<sup>nd</sup> to 6<sup>th</sup> of  
 September)

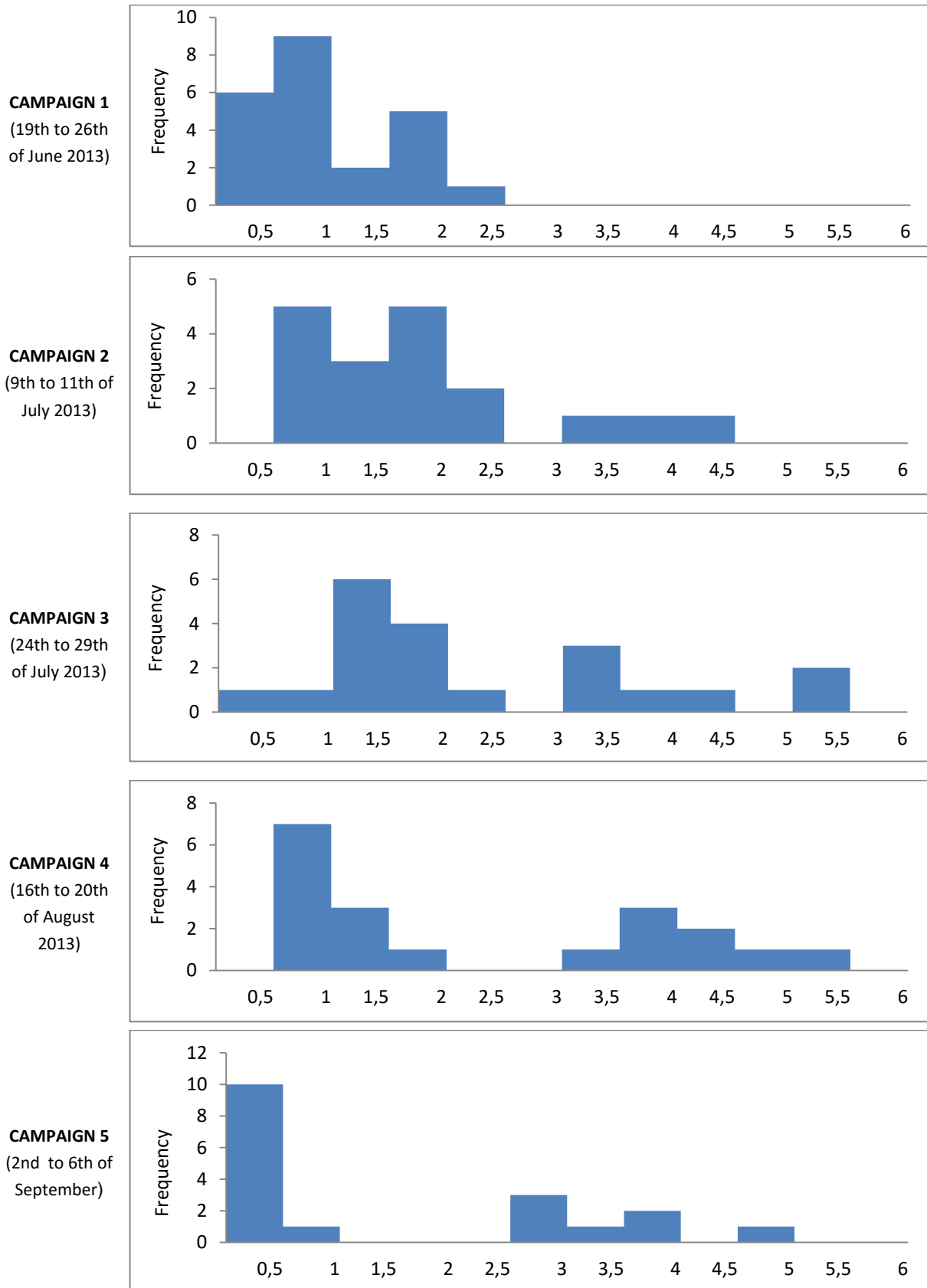




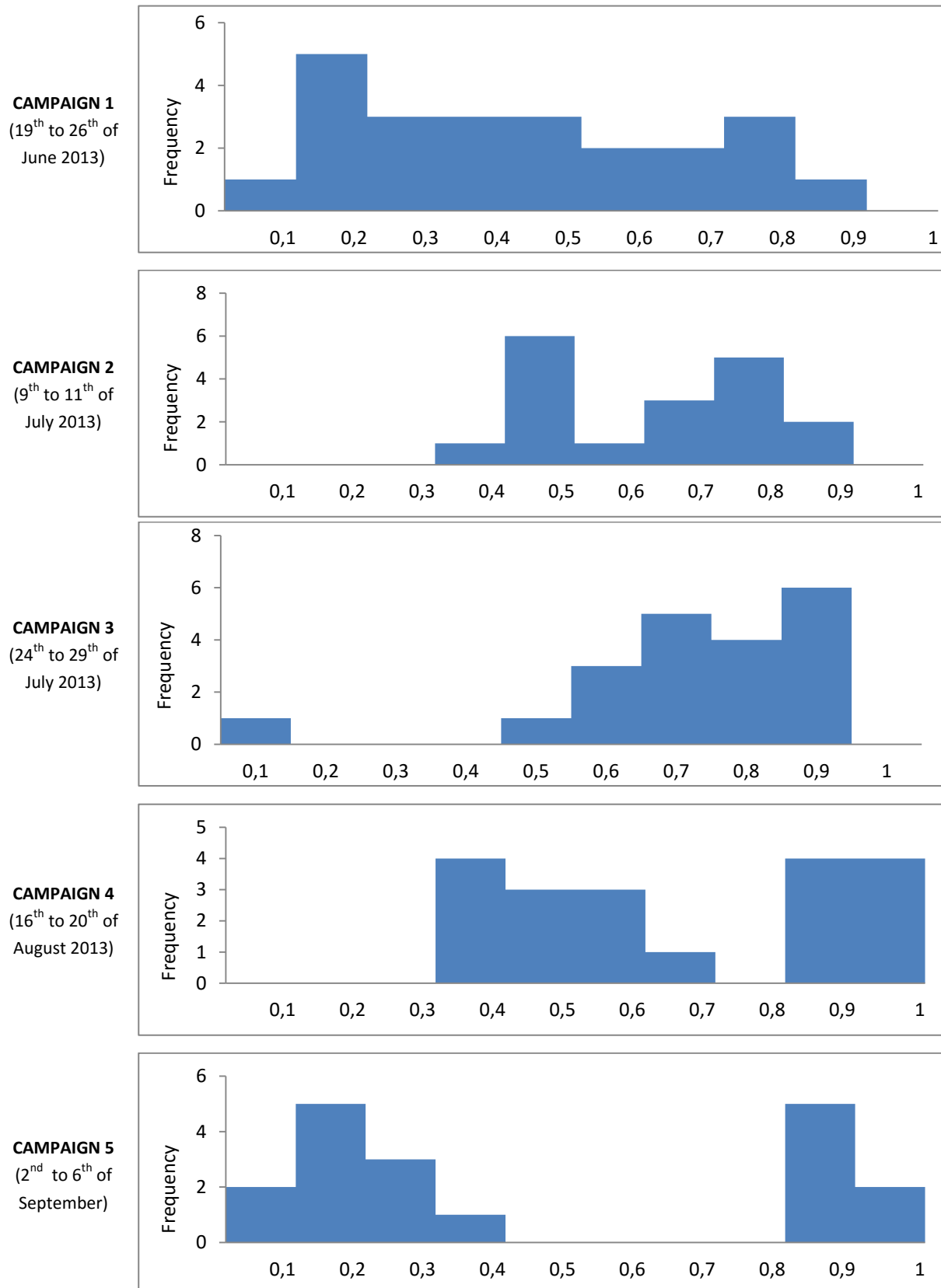
**LAleff**



LAI

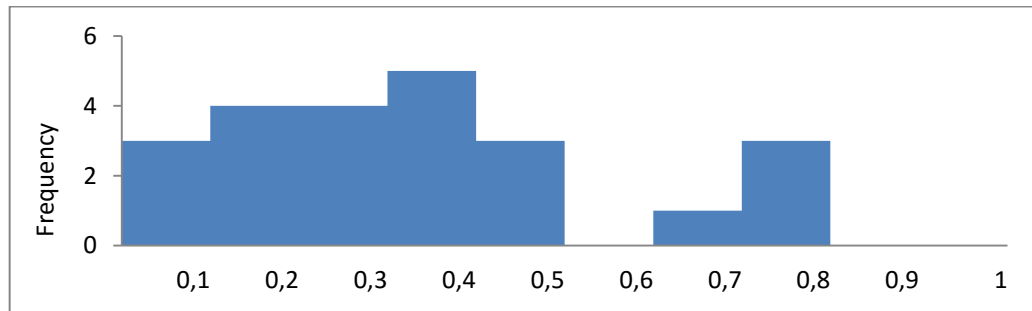


### FAPAR

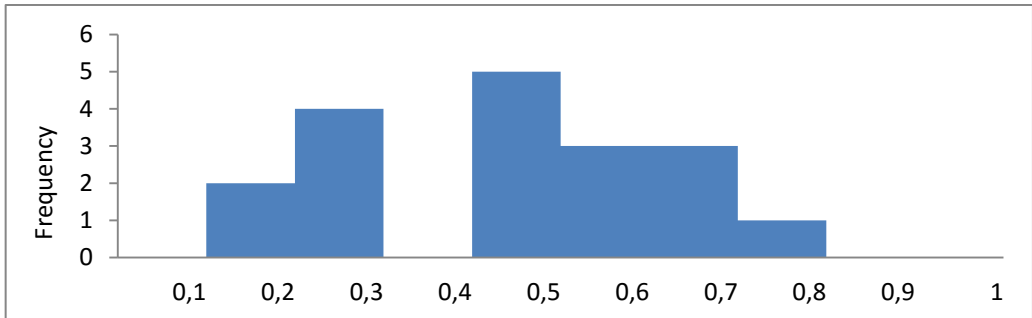


### FCOVER

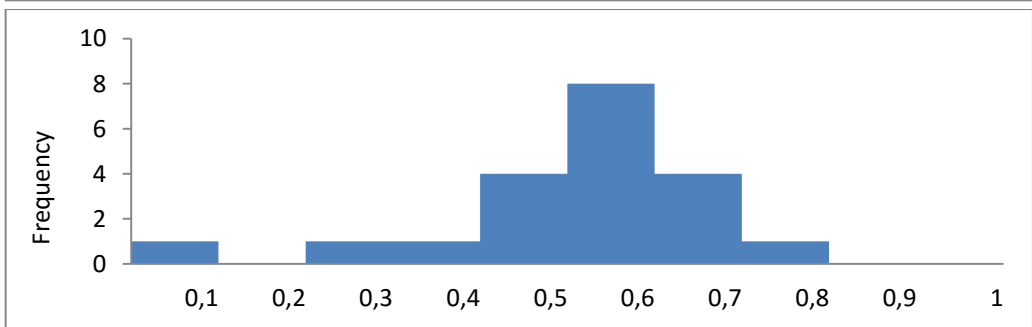
**CAMPAIGN 1**  
 (19<sup>th</sup> to 26<sup>th</sup> of  
 June 2013)



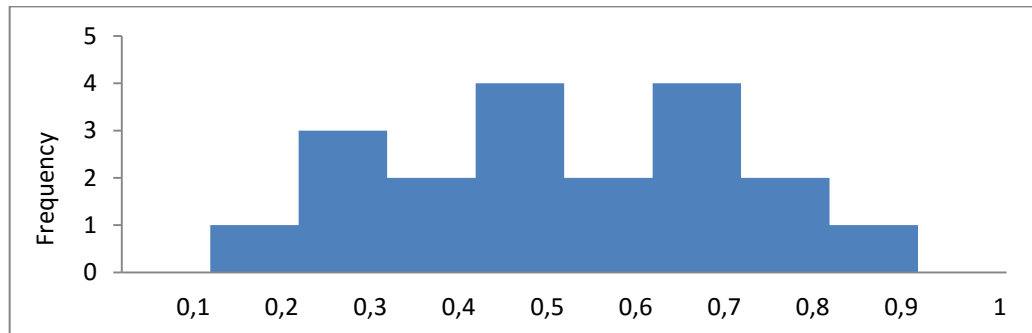
**CAMPAIGN 2**  
 (9<sup>th</sup> to 11<sup>th</sup> of  
 July 2013)



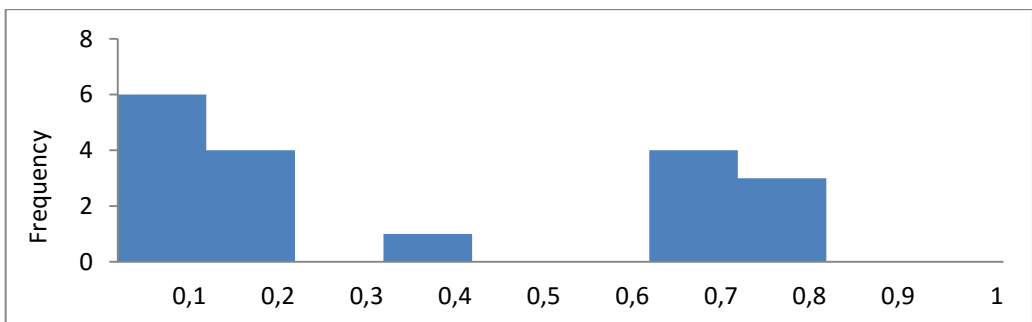
**CAMPAIGN 3**  
 (24<sup>th</sup> to 29<sup>th</sup> of  
 July 2013)



**CAMPAIGN 4**  
 (16<sup>th</sup> to 20<sup>th</sup> of  
 August 2013)



**CAMPAIGN 5**  
 (2<sup>nd</sup> to 6<sup>th</sup> of  
 September)



## ANNEX II: INTERCOMPARISON OF TF RESULTS FOR THE CAMPAIGN THREE BETWEEN SPOT5 AND LANDSAT8

### Acquisition geometry of LANDSAT8 for campaign three

LANDSAT8 METADATA	
Platform / Instrument	LANDSAT_8 / OLI_TIRS
Sensor	OPTICAL 30 m
Spectral Range	B3(green) : 0.53-0.59 $\mu\text{m}$ B4(red) : 0.64-0.67 $\mu\text{m}$ B5(NIR) : 0.85-0.88 $\mu\text{m}$ B6(SWIR1) : 1.58-1.65 $\mu\text{m}$
<b>CAMPAING 3</b> (24 <sup>th</sup> – 29 <sup>th</sup> of July, 2013)	
Acquisition date	2013-07-19
Illumination Azimuth angle	136.324
Illumination Elevation angle	62.063

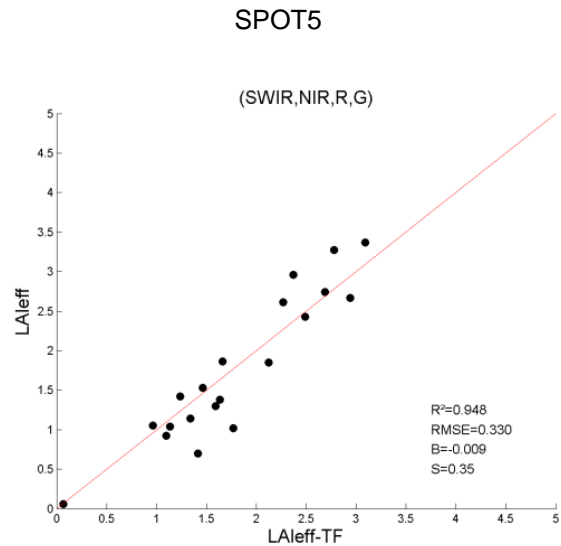
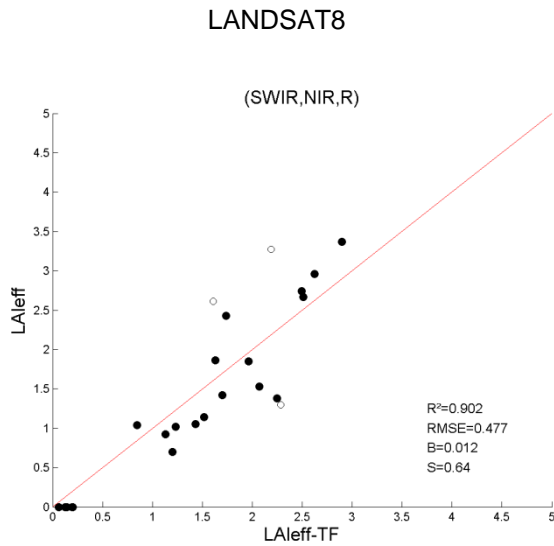
It has been chosen band 2 (Red), band 3 (Near Infrared) and band 4 (Short Wave Infrared). Note that the combination of (2, 3, 4) = (R, NIR, SWIR) is selected for all the parameters in campaign three for LANDSAT8 image.

**Transfer function applied to the whole site for LA<sub>leff</sub>, LAI and FAPAR. RW for weighted RMSE, and RC for cross-validation RMSE for campaign three.**

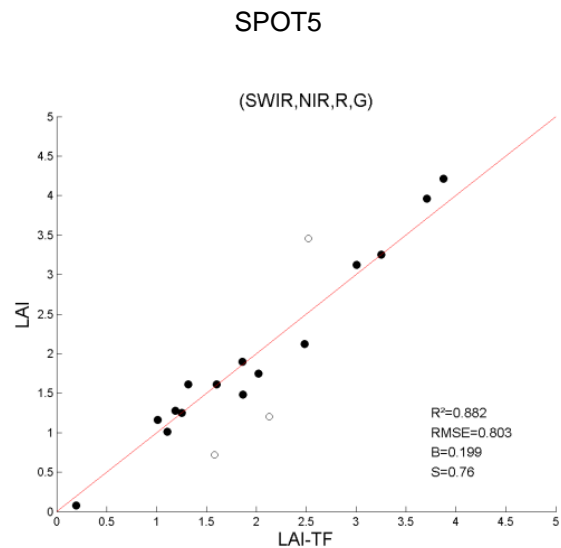
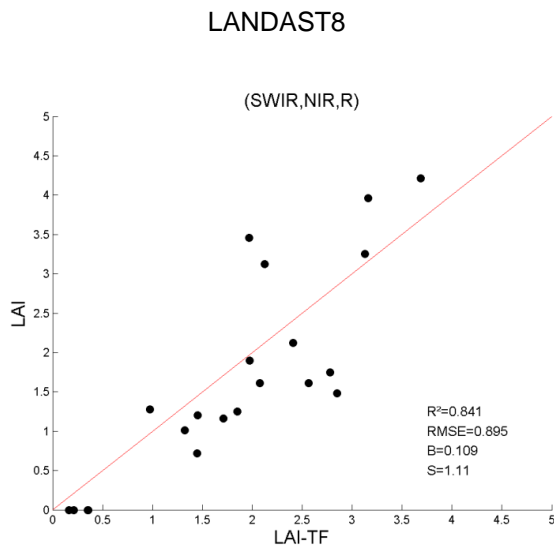
Variable	Band Combination	RW	RC
<b>Campaign three</b>			
<b>LA<sub>leff</sub></b>	-0.39224 -0.00025·(SWIR)+0.00026·(NIR)-0.000006·(R)	0.56	0.57
<b>LAI</b>	-0.99378-0.00037·(SWIR)+0.00035·(NIR)-0.00006·(R)	0.9	1.09
<b>FAPAR</b>	0.17943-0.00003·(SWIR)+0.00006·(NIR)-0.00005·(R)	0.08	0.082
<b>FCOVER</b>	0.12376-0.00002·(SWIR)+0.00005·(NIR)-0.00004·(R)	0.084	0.085

**Intercomparison of scatter plots between LANDSAT8 and SPOT5 images**

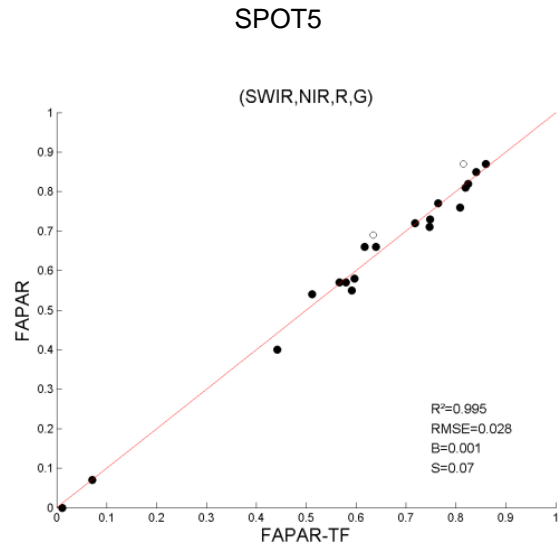
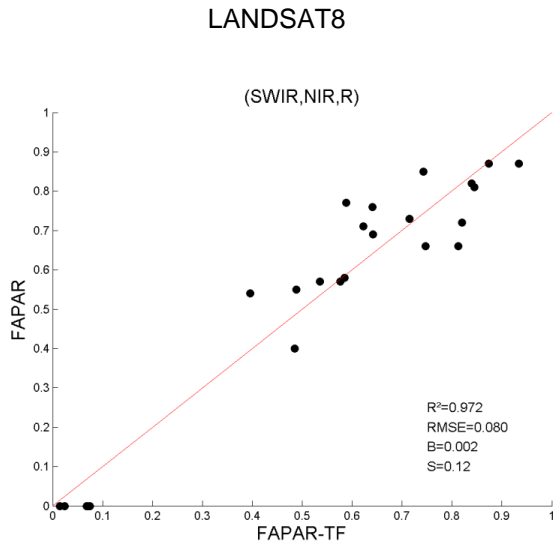
**LAI<sub>eff</sub>**



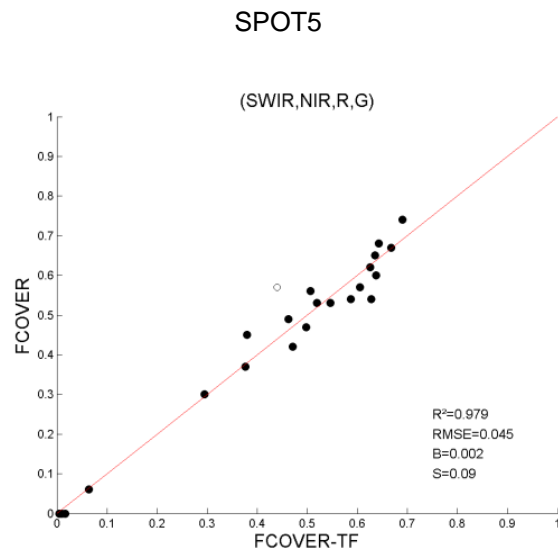
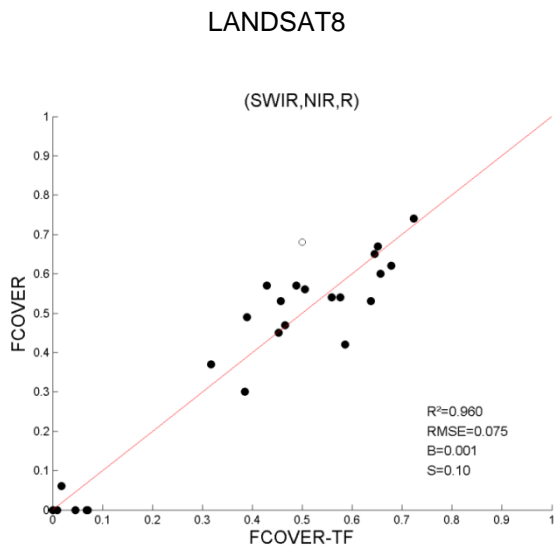
**LAI**



## FAPAR



## FCOVER

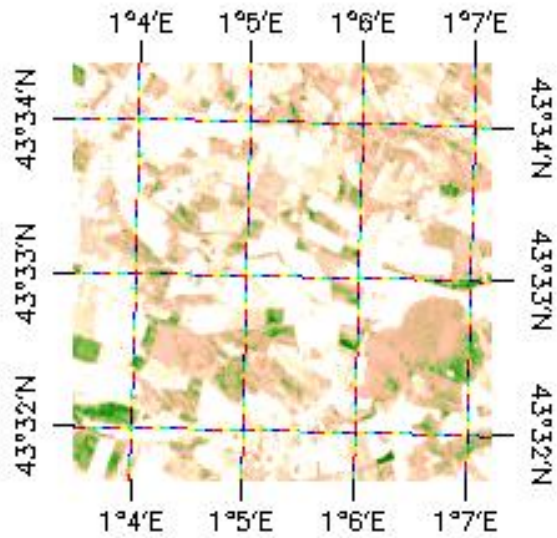




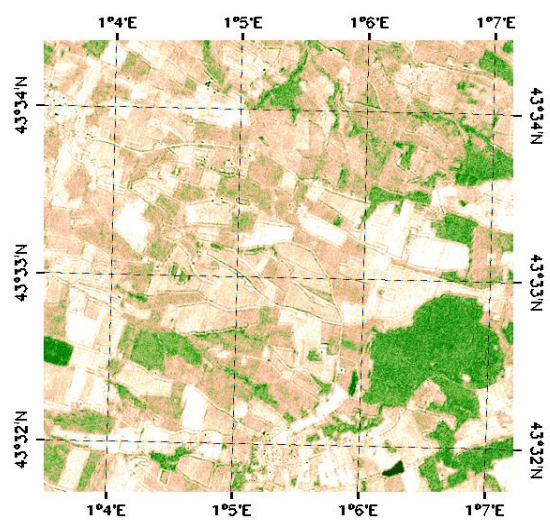
**Intercomparison of ground-based biophysical maps between LANDSAT8 and SPOT5 images applied on the 5x5 km<sup>2</sup> SW1 area for campaign three.**

**LAI**

LANDSAT8

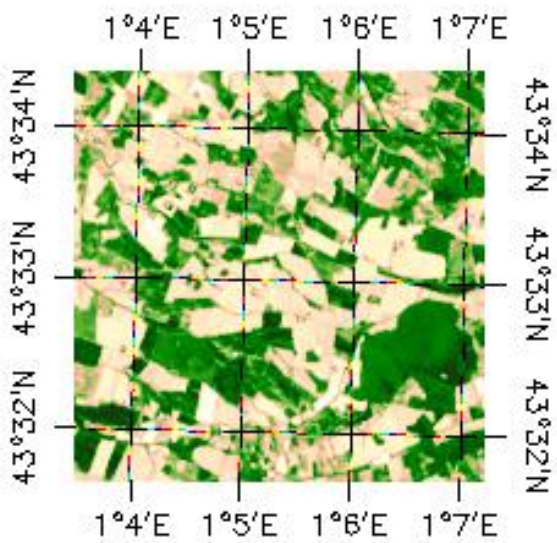


SPOT5

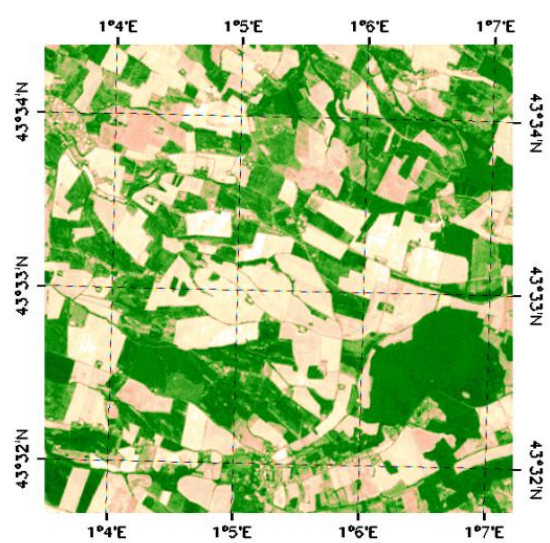


**FAPAR**

LANDSAT8



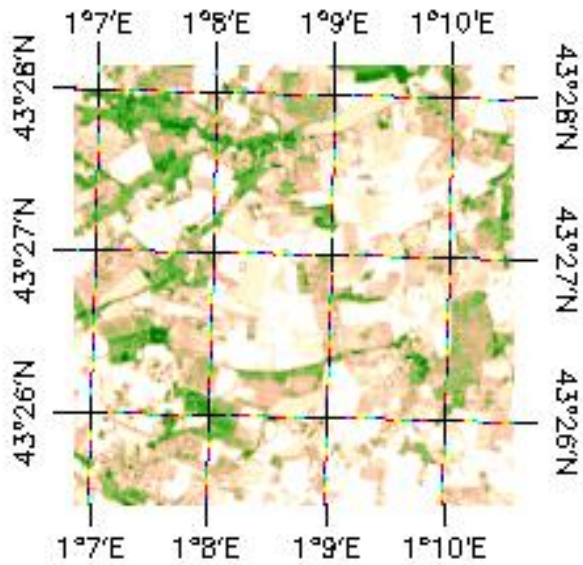
SPOT5



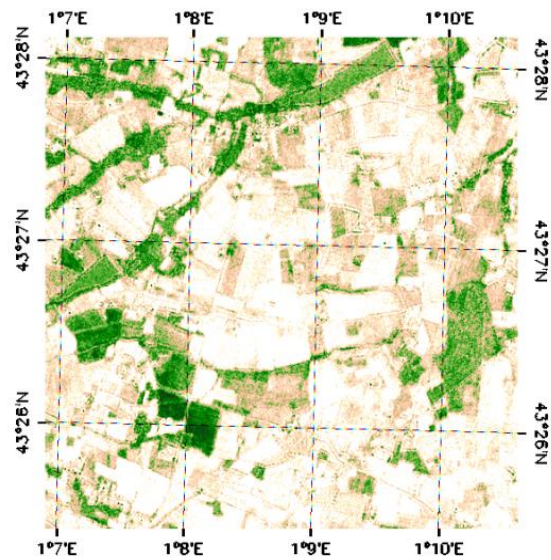
**Intercomparison of ground-based biophysical maps between LANDSAT8 and SPOT5 images applied on the 5x5 km<sup>2</sup> SW2 area for campaign three.**

**LAI**

LANDSAT8

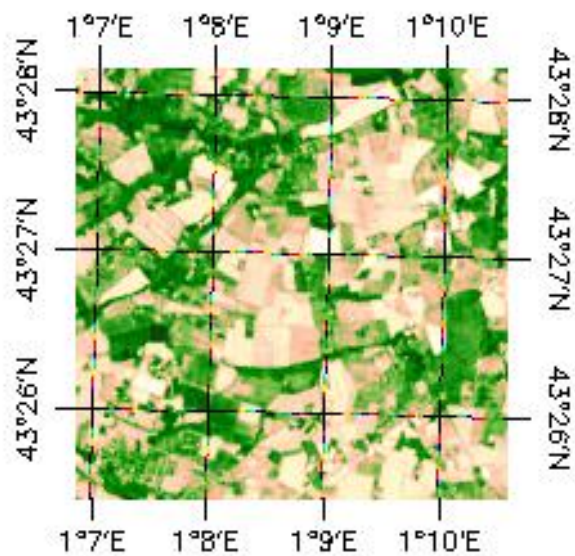


SPOT5

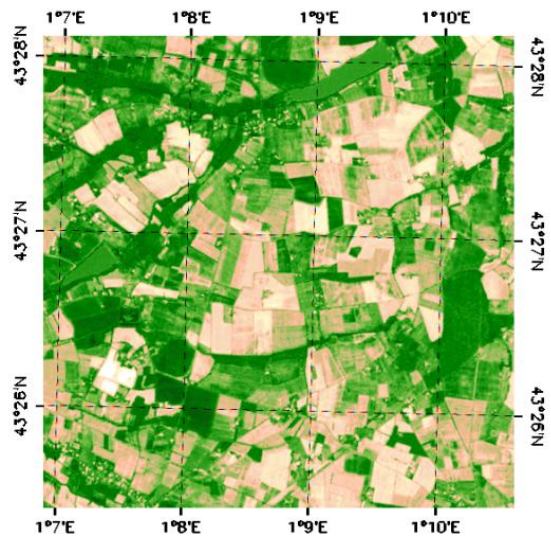


**FAPAR**

LANDSAT8



SPOT5



**Intercomparison of mean values between LANDSAT8 and SPOT5 images of the HR biophysical maps for the 3x3km<sup>2</sup> SW1 area**

<b>SW1 ( 43.5511N 1.08889E)</b>		
	<b>LANDSAT8</b>	<b>SPOT5</b>
<b>LAI<sub>eff</sub></b>	1.03	1
<b>LAI</b>	1.23	1.19
<b>FAPAR</b>	0.40	0.39
<b>FCOVER</b>	0.33	0.32

**Intercomparison of mean values between LANDSAT8 and SPOT5 images of the HR biophysical maps for the 3x3km<sup>2</sup> SW2 area**

<b>SW2 ( 43.44708N 1.14504E)</b>		
	<b>LANDSAT8</b>	<b>SPOT5</b>
<b>LAI<sub>eff</sub></b>	0.84	0.67
<b>LAI</b>	0.90	0.69
<b>FAPAR</b>	0.40	0.46
<b>FCOVER</b>	0.32	0.36